

1 **Seismogenic Fault Reactivation in Western Central Africa: Insights**
 2 **from Regional Stress Analyses**

3 **Hardy Medry Dieu-Veill Nkodia¹, Timothée Miyouna¹, Folarin Kolawole^{3,4}, Florent**
 4 **Boudzoumou^{1,2}, Alan Patrick Rodeck Loemba¹, Nicy Carmel Tchiguina Bazebizonza¹,**
 5 **Damien Delvaux⁵**

6
 7 ¹Marien NGOUABI University, Faculty of Sciences and Technics, Department of Geology, B.P.
 8 60, Brazzaville, Republic of Congo.

9 ²National Research Institute in Exact and Natural Sciences of Brazzaville, P.O. 2400, Republic of
 10 Congo (IRSEN).

11 ³Lamont-Doherty Earth Observatory, Columbia University, 61 Rte 9W, Palisades, NY, United
 12 States.

13 ⁴BP America, 501 West Lake Blvd., Houston, TX, United States.

14 ⁵Department of Geology, Royal Museum for Central Africa, Leuvensesteenweg 13, B-3080
 15 Tervuren, Belgium.

16 Corresponding author: Hardy Medry Dieu-Veill Nkodia¹ (nkodiahardy@gmail.com).

17
 18 **Key Points:**

- 19 • A transpressive regime with NNE-SSW horizontal maximum compressive stress controls
 20 intraplate seismicity in Western Central Africa
- 21 • Regional stresses acting on offshore oceanic fracture zones are compatible with those
 22 acting along the onshore continental margin.
- 23 • Favorable orientation and hydrothermal alteration of onshore preexisting Archean -
 24 Cenozoic faults make them susceptible for reactivation.
 25

Abstract

The onshore continental margins of western Central Africa have been hosting potentially damaging earthquake events for decades; yet, the links between the seismicity, the contemporary stress field, and pre-existing faults are not well understood. Here, we analyze the regional stress fields along the coastal margin and interior cratonic areas using earthquake focal mechanisms, map and characterize the detailed structure of preexisting fault systems in outcrops, and assess the reactivation potential of the mapped structures. Our results show that the earthquakes originate under a transpressive stress regime with a horizontal maximum principal compressive stress (σ_1) that is oriented NNE-SSW. We show that regional stresses acting on offshore oceanic fracture zones are compatible with those acting along the onshore areas of the continental margin. Field observations reveal the presence of large fault systems that deform both the Precambrian basement and Phanerozoic sedimentary sequences, with widespread hydrothermal alterations of calcite veining, quartz veining, and palygorskite mineralization along the fault zones. Along the margin, the preexisting NNE-, NNW-, and N-S -trending strike-slip faults and normal faults show a high slip tendency (60 – 100 %), whereas in the cratonic interior, the NW- and N-S -trending thrust faults are the most likely to reactivate. We argue that favorable orientation of the preexisting faults and potentially, their hydrothermal alteration products, define the susceptibility of the faults to seismic reactivation. We propose that possible stress propagation into the near-shore and onshore tip zones of oceanic fracture zones may be driving stress loading on pre-stressed fault systems onshore.

Keywords: Earthquakes, Intraplate seismicity; Slip tendency; faults; Western Central Africa; focal mechanism.

Plain Language Summary

We investigated the stresses that are generating earthquakes and the compatibility with preexisting fault systems along the stable continental margin of Western Central Africa. The stresses acting on the continent interior were also determined and distinguished. We found that the regional stresses acting on offshore oceanic fracture zones are compatible with those acting along the onshore areas of the continental margin. In this stress field, the potential for reactivation of the observable preexisting onshore fault systems is very high, particularly for those oriented NNE-SSW and N-S. We propose that the stresses along transform faults and oceanic fracture zones may propagate into near-shore and onshore areas, leading to earthquakes on the preexisting faults.

58
59

60 1 Introduction

61 Earthquakes remain one of the most catastrophic natural hazards in human history. Beyond the
62 associated fatalities, earthquakes also leave behind lasting environmental and economic crises in
63 the affected communities. Although, the largest magnitude earthquakes have been recorded along
64 plate boundaries (McCaffrey, 2008) associated with plate subduction, collision, and continental
65 rifting, several large magnitude ($M_w > 6$) events have also been recorded in intraplate regions
66 (e.g., Talwani, 2014; Tuttle et al., 2002), and more intriguingly, along passive continental rift
67 margins where the sources and occurrence of earthquakes remain less understood. Among the large
68 magnitude and devastating earthquakes recorded in continental intraplate regions previously thought
69 to be relatively stable include the M_w 6.2 Latur Earthquake of September 29, 1993 in South India
70 which claimed a death toll of 11,000 (Gupta et al., 1998) and the M_w 6.2 Guinea earthquake of
71 December 22, 1983 which caused 1500 fatalities and significant property damage (Musson, 1992;
72 Suleiman et al., 1993). On the causes of intraplate seismicity, proposed hypotheses include the
73 reactivation of preexisting structures (e.g., Calais et al., 2016; F. Kolawole et al., 2019; Folarin
74 Kolawole et al., 2017; Ngatchou et al., 2018) driven by far-field stress transmission from active
75 plate boundaries (Delvaux et al., 2016; Delvaux & Bath, 2010; Nkodia et al., 2020; Wiens & Stein,
76 1983, 1985), gravitational body forces (Levandowski et al., 2017), deglaciation-related isostatic
77 rebound (Lund Snee & Zoback, 2020), underground industrial activities (Grigoli et al., 2017;
78 Keranen & Weingarten, 2018), and thermal weakening of the lithosphere (Holford et al., 2011).
79 Some passive rifted margins across the world are known host pronounced distributed seismicity,
80 among which are well-instrumented regions such as the eastern Brazilian Atlantic margin
81 (Assumpção, 1998), the southern Australian margin (Holford et al., 2011), and the eastern North
82 American margin (Sbar & Sykes, 1973; Zoback, 1992). However, in poorly instrumented regions,
83 such as Equatorial West Africa and western Central Africa where widespread seismicity is
84 becoming increasingly prominent, the relation between the present-day stress regime acting in
85 these regions, the sources of stress perturbation, and the mechanics of reactivation of inherited
86 structures are not known (Olugboji et al., 2021). This knowledge gap hinders the development of
87 viable early-warning mechanisms for hazard mitigations in local communities located in such
88 regions.

89 In this study, we explore the passive margin of Western Central Africa, an area which exemplifies
90 considerable intraplate seismicity in both its offshore domains and within the continent (Figs. 2a-
91 b). This region has been the subject of much research for almost a century (Krenkel, 1923; Junner
92 and Bates, 1941; Blundell, 1976; Burke, 1976; Bacon and Quaah, 1981; Ambraseys and Adams,
93 1986; Yarwood and Doser, 1990; Onuoha and Ezeh, 1992a; Musson, 1992; Suleiman et al., 1993;
94 Delvaux and Bath, 2010; Amponsah et al., 2012; Kutu, 2013; Nwankwoala and Orji, 2018;
95 Meghraoui et al., 2019; Oladejo et al., 2020; Olugboji et al., 2021; Kadiri and Kijko, 2021).
96 Although most of the studies focused on the use of remote sensing to provide a seismotectonic
97 model for the region (Adepelumi et al., 2008; M. O. Awoyemi et al., 2017; M. Awoyemi &
98 Onyedim, 2004; Bouka Biona & Souna, 2001; Oladejo et al., 2020), the characterization of the
99 structures is sparse, and there remains a limited understanding of the detailed structure and current
100 stress state of the potentially-seismogenic preexisting faults.

101 The aim of this contribution is to evaluate the possible current regional stress regime that is most
102 dominant and is responsible for reactivating preexisting structures along the western Central
103 African passive margin by using the slip tendency analytical techniques. By determining which
104 types of structures that are being reactivated within the study area and the associated kinematics,
105 we provide some insight into the seismic hazards and possible drivers of widespread seismicity

106 along the margin. We suggest that the results of this study are relevant for building a realistic
107 model for seismic hazards and the associated coseismic ground motions for this region and
108 similar poorly-instrumented passive margin environments:
109

110 **2 Geological and Tectonic Setting**

111 **2.1 Regional Geology of Western Africa and Continental Margin**

112 The Western Africa continental region is mainly dominated by Archaean basement, overlain by
113 Neoproterozoic and Phanerozoic units (Fig. 1). The Archean rocks are hosted within the Congo
114 Craton in the western Central Africa region and in the West African Craton in the far northwestern
115 sub-region. These cratons are separated into several blocks limited by Neoproterozoic and
116 Paleoproterozoic terranes and shear zones, interspersed by sedimentary basins (Fig. 1). The 3.1 -
117 2.7 Ga Congo Craton (Thiéblemont et al., 2009; Turnbull et al., 2021) is subdivided into five
118 blocks: (i) the Ntem-Chaillu block in the central and northwestern domains, covering the region
119 of Cameroon, Gabon, and Republic of Congo (Kessi, 1992; Tchameni et al., 2000; Gatsé
120 Ebotehouna et al., 2021a); (ii) the 2.5 Ga Angola block to the south in Angola (De Carvalho et al.,
121 2000; Jelsma et al., 2018); (iii) the 3.6 - 2.5 Ga Kassai block to the southeast in DRC (Batumike
122 et al., 2006); (iv) the 3.2 - 2.5 Ga NE-Congo Block in the Northern DRC (Turnbull et al., 2021),
123 and (v) the 2.8 - 2.6 Ga Tanzanian block.

124
125 These cratonic blocks have accommodated multiple episodes of large-scale brittle deformation
126 which emplaced large discontinuities within them. Akame et al., (2020, 2021) documented the
127 presence of large NW-SE, NE-SW and E-W trending brittle and ductile shear zones in the Ntem-
128 Chaillu Block, inherited from Neoproterozoic orogenesis. Similar deformation were also reported in
129 the laterally equivalent Souanké Archean rocks in the Ivindo region of Republic of Congo
130 (Loemba et al., 2022) In the Souanké domain, the brittle shear zones show evidence of reactivation
131 into normal faulting kinematics interpreted to be related the Cretaceous opening of Atlantic Ocean
132 (Loemba et al., 2022). The Ntem-Chaillu block is bounded to the north by the Oubanguides Belt
133 which developed during the Pan-African Orogeny (550 ± 100 Ma) and was subsequently deformed
134 in the Mesozoic by the continental-scale, NE-trending Central African Shear Zone (CASZ; Fig.
135 1). The CASZ, which extends into the Borborema province of NE Brazil (Miranda et al., 2020), is
136 considered to be an accommodation zone that was activated during the opening of the South
137 Atlantic (Moulin et al., 2010; V. Ngako et al., 2003; Vincent Ngako et al., 1991; Njonfang et al.,
138 2008; Wilson, 1965). Recent earthquakes and associated source mechanisms along a segment of
139 the CASZ (e.g., 2005 Montalé, Cameroon earthquake) suggests that the CASZ structure may still
140 be active as the Atlantic Ocean basin continues to open (Ngatchou et al., 2018).

141 Along the western margin of the Congo Craton, the Ntem-Chaillu and Angola cratonic blocks are
142 separated by the Pan-African West-Congo Belt (630 Ma – 490 Ma) the western part of which was
143 later rifted during the opening of the Atlantic Ocean (Alvarez & Maurin, 1991; Boudzoumou &
144 Trompette, 1988; Bouenitela, 2019; Fullgraf et al., 2015; Hossié, 1980). The fold-thrust terranes
145 of the West-Congo Belt is noted to host large (>90 km-long) NE-SW, NW-SW and N-S trending
146 brittle shear zones (Alvarez & Maurin, 1991; Nkodia et al., 2021). In the Republic of Congo (RC),
147 Democratic Republic of Congo (DRC), and Angola, the terranes of the mobile belt are covered by
148 Ordovician-Silurian sandstones which record phases of strike-slip deformation, first during the
149 Gondwanide Orogeny in the Permo-Triassic, then during Cretaceous opening of the Atlantic

150 (Miyouna et al., 2018; Nkodia et al., 2020). The Late Paleozoic sandstones of the Inkisi Group
 151 show reactivated and segmented strike-slip faults zones oriented NW-SE, NE-SW, and E-W,
 152 observable in field outcrops (Miyouna et al., 2018; Nkodia et al., 2020a) and in seismic reflection
 153 images (Damien Delvaux et al., 2021; Kadima et al., 2011). The phases of Late Paleozoic-Early
 154 Mesozoic contractional tectonic deformation in the Congo Basin are observable across eastern and
 155 southern Africa (Delvaux et al., 2021) However, there is evidence for the presence of through-
 156 going structures which deform both the Paleozoic-Mesozoic and Cenozoic sedimentary sequences
 157 (Damien Delvaux et al., 2021; Kadima et al., 2011), suggesting there might be still be on-going
 158 intra-continental tectonic deformation in Central Africa. Mbéri Kongo (2018) showed that the
 159 Paleogene sand deposits of the Bateké Plateau, Congo Basin, have been deformed by large strike-
 160 slip faults with associated conjugate normal faults. Northwest of the Oubanguides Belt, in West
 161 Africa, the Cretaceous intracratonic Benue Rift developed within the Trans-Sahara Mobile Belt as
 162 a corridor of transtensive faults with associated magmatism (Ajakaiye et al., 1986; Benkhelil,
 163 1989; Oha et al., 2020). The closure and failure of the rift occurred in the Santonian, associated
 164 with a transpressional deformation of its Cretaceous syn-rift deposits (Ofoegbu, 1985; Benkhelil,
 165 1989). The Trans-Sahara Mobile Belt host several N- to NNE-trending shear zones associated with
 166 the Proterozoic amalgamation of West Gondwana. Some of the shear zones also record evidence
 167 of brittle deformation during the opening of the Atlantic Ocean, an example of which is the Kandi
 168 fault zone which served as an accommodation zone during the rifting event (Affaton et al., 1991).

169
 170 **Figure 1:** Map of the bedrock geology of the Nubian Plate showing major litho-tectonic subdivisions of the
 171 crust. Dwcl, Dk, Dbk, Dngov, Dso represent field sites where structural measurements of fault systems
 172 were collected. Dwcl represent the study site of a thrust fault system in western Congo. Dwc2 is a
 173 combination of strike-slip faults along Dk and Dngov which represent field sites in Kolas Quarry, Republic
 174 of Congo, and Ngovo Cave, Democratic Republic of Congo respectively. Dbk represents the field study
 175 sites of fault systems in Brazzaville and Kinshasa areas. AFZ: Akwapim Fault Zone, BFZ: Bouandary Fault
 176 Zone, CASZ: Central African shear zone.

177

178

179 **2.2 Oceanic Fracture Zones in the Gulf of Guinea, Western Nubian Plate**

180 The oceanic crust of the Atlantic Basin dominates the western portion of the Nubian Plate and
 181 hosts several fracture zones that extend eastward from the active transform faults at the Mid-
 182 Atlantic Ridge plate boundary towards western Africa's rifted continental margin (Fig. 1). Oceanic
 183 transform faults developed within the oceanic crust starting sometime after continental break-up
 184 and serve to accommodate the lateral movement of tectonic plates, and lateral variation of
 185 spreading rates, and to facilitate connectivity between ridges and trenches (De Long et al., 1977,
 186 p. 199; Gerya, 2012; Hensen et al., 2019). Due to their strong topographic expression at the sea
 187 floor, their structural and geochemical alteration of the oceanic crust, and temporal accretion
 188 patterns, transform faults and oceanic fracture zones are mappable in bathymetric, seismic
 189 reflection, gravity, and magnetic datasets (Delteil et al., 1974; Fail et al., 1970; Gorini & Bryan,
 190 1976; Guiraud et al., 2010; Mascle & Sibuet, 1974).

191 Although the active plate boundary (i.e., spreading oceanic ridges and subduction zones) host most
 192 of the seismicity of oceanic basins, oceanic fracture zones and their flanking areas also
 193 accommodate significant seismic activity and represent seismic hazards within intraplate areas
 194 away from the plate boundaries (Fig.2a; Burke, 1969; Lay, 2019; Okal & Stewart, 1982). On the

195 lateral growth of oceanic fracture zones, Burke et al. (1969) proposed a mechanism of propagation
196 towards the continents by extension fracture mode which produce stress transmission that initiate
197 seismic failure at the continental margins. In the Atlantic Ocean, some of the most active fracture
198 zones which commonly extend close to- or into the western Africa rifted continental margin
199 include Romanche, Chain, Charcot, Ascension, and Saint Paul fracture zones (Figs. 2a-b; Heezen
200 et al., 1964, 1965; Mascle & Sibuet, 1974). A few studies argue for the lateral continue of oceanic
201 fracture zones onto the continent of West Africa and causative relationship with onshore
202 earthquakes based on: 1) the alignment of on-shore magnetic lineaments in Nigeria with the trends
203 of the offshore fracture zones (Ajakaiye et al., 1986), and 2) the colocation and alignment of rifted
204 transform margins such as the Ghanian and Ivorian coastline with the Romanche and St Paul
205 fracture zones respectively (Fig. 2a; Antobreh et al., 2009), and 3) recent (<10 million years)
206 acceleration of strain rates on oceanic transform faults post-continental break-up in the Late
207 Cretaceous (Meghraoui et al., 2019). However, questions remain on the link between the current
208 stress regime acting on the margin of western African continent and the mechanisms and triggers
209 of seismic reactivation of preexisting structures.

210

211 **3 Data and Methods**

212 **3.1 Earthquake Data**

213 The study area covers the region between latitudes 16.70°N and 14.07°S, and longitudes 23°W
214 and 24.66°E. For this region, we built a database of earthquakes and their related focal mechanism
215 data from publicly-accessible global catalogues which includes the International Seismic Center
216 (ISC), the United States Geological Survey (USGS), the Global Centroid-Moment-Tensor (CMT),
217 and the GFZ GEOFON earthquake catalogs.

218

219 **3.2 Mapping of Tectonic Lineaments**

220 In order to delineate mega-scale tectonic structures in the oceanic crust and around the onshore
221 continental coastal margin, we utilized hillshade digital elevation model (DEM) maps generated
222 from bathymetric and topographic data. In the offshore areas, we delineated and mapped the traces
223 of oceanic fracture zones on DEM of bathymetric data extracted from GEBCO (GEBCO
224 Bathymetric Compilation Group 2021, 2021), which has a spatial resolution of 1 arc minute (~1.5
225 km). Within the onshore continental areas, using previously published geologic maps and field
226 observation where possible (see details in section 3.3) as constraints, we manually interpreted and
227 digitized visible structural lineaments defined by steep laterally-continuous topographic relief
228 gradients from a mosaic of scenes of a 30 m resolution ALOS-type radar interferometric digital
229 elevation model (DEM) images, following a standard approach (Burbank & Anderson, 2011). The
230 ALOS data was obtained from the ALOS Global Digital Surface Model
231 (<https://www.eorc.jaxa.jp/ALOS/en/aw3d30/data/index.htm>). The previously published geologic
232 map that guided the lineament interpretation is the tectonic map of Africa by Milesi et al. (2010)
233 in which the faults were compiled from field studies and gravity anomalies, conducted by
234 geological surveys groups of different countries.

235

236 **3.3 Field Observations and Collection of Structural Measurements**

237 In the onshore areas of the Republic of Congo (R.C) and Democratic Republic of Congo (D.R.C),
238 we conducted field observations and collection of structural data along the fault and fracture
239 systems in outcrops. This field campaign also served as ground-truthing to constrain the mapping
240 of structural lineaments in hillshade maps. The field campaigns were conducted in the regions of
241 Brazzaville, Dolisie, and Souanké regions of R.C, and in the Kongo Central region of D.R.C. The
242 fieldwork helped to confirm the geologic origin of some of the interpreted lineaments as fault
243 strands or brittle shear zones where they are accessible. In the field outcrops of the faults and brittle
244 shear zones, we collected measurements of strike and dip of fault planes, trend and plunge of slip
245 vectors (striations) along the surfaces, and we documented evidence and characteristics of
246 geochemical alterations of the fault zones. We have provided information on our field
247 measurements in the supplementary file of this manuscript. The structural field measurements
248 provide fault plane orientation data that we used as one of the inputs into the slip tendency analysis
249 (see section 3.4).

250

251 **3.4 Assessment of Contemporary Stress Field and Slip Tendency of the Preexisting Structures**

252 Following a standard approach, we used the Win-Tensor program (D. Delvaux, 2012) to determine
253 the current stress field acting on the Gulf of Guinea section of the Nubian Plate, using the
254 information on source parameters of earthquake focal mechanism solutions as input data. The focal
255 mechanism solution data were compiled from several literature review (see supplementary files),
256 Global CMT moment tensor, and GFZ GEOFON earthquake catalogs (Fig. 2b). In cases where
257 the focal mechanism solution of the same earthquake event is produced by multiple earthquake
258 databases, we considered all the solutions in order to guarantee the precision of the resulting stress
259 tensor solutions. For our analysis, since the available focal mechanism solutions are sparse across
260 the region and the seismicity is distributed across 1) offshore and onshore areas along the coastal
261 margin corresponding to a rifted tectonic domain and the underlying pre-rift Proterozoic mobile
262 belt, and 2) an Archean cratonic interior that has experienced failed rifting and inversion, we
263 divided the study region into three sub-regions defined by three boxes (sub-regional Boxes 1, 2,
264 and 3 in Fig. 3b). The division was made by considering the assumption that each box has a
265 uniform stress. Two boxes cover the coastal margin areas: one along the Gabon-Cameroon and the
266 other along the Ghanaian coastal margins; whereas the third box covers the cratonic continental
267 interior of central Africa.

268 The Win-Tensor program uses the stress inversion method (Angelier, 1975, 1989; Angelier &
269 Mechler, 1977) to determine a reduced tensor which contains the orientations of the principal
270 compressive stress axes (σ_1 , σ_2 , and σ_3) and the stress ratio, R. The program first estimates the
271 tensor solution using the determination of PBT (compression, intermediate and tensional) axes
272 method and the Right Dihedron method. This initial stress tensor solution serves as a starting point
273 to determine a more constrained tensor solution using an iterative Rotational Optimization method.
274 The latter method uses a misfit function that minimizes the difference between the calculated slip
275 direction and the resolved direction. Fault planes that show large misfit angle are rejected in order
276 to have a better constrained result. The stress index regime, R', typified the regime associated with
277 the solution tensor. R' is an improved R ratio that gives the type of stress regime in a continuous
278 scale of 0 to 3 (Fig. 2).

279

280

281 **Figure 2:** Standard values of the stress index R' with respect to the stress regime (modified from Delvaux
 282 et al., 2017).

283
 284 The resultant tensor solutions from Box 1 and Box 2 were applied on the mapped fault systems in
 285 central Africa to determine the slip tendency of the different observed fault plane geometries. Note
 286 that we do not use the tensor solution for Box 3 because it is similar to that of Box 1 (see section
 287 4.3). Slip tendency quantifies the potential for reactivation of fault planes under a given stress field
 288 (Morris et al., 1996). The magnitude of slip tendency depends on the ratio of shear stress to normal
 289 stress resolved on a fault or fracture surface, and the frictional characteristic of the rocks. The Win-
 290 Tensor program determines a normalized slip tendency (Tsn) (Lisle & Srivastava, 2004) rendered
 291 as continuous values in a colored scale of 0 to 1. The planes with a slip tendency above 0.6 are
 292 considered to have a high likelihood to be reactivated, and less likely are the planes below 0.6. For
 293 our analysis, we use 0.3 as the coefficient of friction according to the work of Angelier (1989). We
 294 assume a cohesionless residual strength envelope for the faults, defined by 0 MPa cohesion, based
 295 on the outcrop observation of widespread brittle reactivation of hydrothermally-altered fault zones
 296 (see section 4.2).

297

298 **4 Results**

299 **4.1 Spatial Distribution of Earthquakes and Mapped Tectonic Lineaments**

300 Offshore, seismic events are either collocated with or occur in the vicinity of traces of oceanic
 301 fracture zones which show dominant trends of ENE and NE (Fig. 3a). Some events also occur
 302 along the Cameroon volcanic line and around the Bié Dome in Angola. However, onshore, along
 303 the coastal margin and continental interior areas, the regional seismicity patterns show clustering
 304 of events that are collocated with or in vicinity of the mapped tectonic lineaments (Fig. 3a). For
 305 example, at the location of field site Dso, the epicenter of a Mw 6 event is collocated with the trace
 306 of a large ENE-to-NE trending fault system in the Ntem-Chaillu Block (see lineament with label
 307 'Dso' in Figs. 1 and 3a). More interestingly, earthquakes cluster at the location where the
 308 Romanche Fracture Zone extends onto the Ghanian shoreline (Fig. 3a); and at least one of each of
 309 the nodal planes on the associated focal mechanism solutions show a trend that is parallel or sub-
 310 parallel to the fracture zone orientation (Fig. 3b). In southern Ghana and surrounding regions,
 311 tectonic lineaments show dominant sets trending NNE and ENE of which the latter is parallel to
 312 the trend of the Romanche Fracture Zone (Fig. 3a). Most of the focal mechanism solutions of the
 313 earthquakes (Fig. 3b) show a dominance of thrust fault and strike-slip fault regime. Only 10 % of
 314 events show normal faulting regimes (pie chart in Fig. 3b) and most are restricted to the rifted
 315 costal margin. Within the continental interior, the strike-slip and reverse faulting regime appear to
 316 be distributed across a broad region.

317

318 **Figure 3:** (a) Relief map showing the distribution of earthquakes in the Western Africa passive margin.
 319 AFZ, CASZ are the Akwapim Fault zone, the Central Africa shear zone. (b) Focal mechanism solutions for
 320 earthquakes in the western part of the Nubia Plate, obtained from several literature review, Global CMT
 321 moment tensor, and GFZ GEOFON earthquake catalogs. The boxes show the area where conducted stress
 322 inversion on focal mechanism results. The pie-chart show the frequency distribution of the different tectonic
 323 regime acting on the area. TS: trenstensional regime; NF: normal faulting regime; SS: strike-slip faulting
 324 regime; TF: thrust faulting regime.

325

326 **4.2 Fault Structure in the Field Outcrops**

327 The study area is dominantly affected by strike-slip faults trending NW-SE, NE-SW, and minor
 328 ENE-WSW to E-W. Locally, these regions showed thrust faults and normal faults settled during
 329 Pan-African orogenies, post-Pan-African and the opening of Atlantic Ocean. At the field sites in
 330 Republic of Congo (RC) and Democratic Republic of Congo (DRC), observable deformation in
 331 the Paleozoic sandstones of the Inkisi Group mostly showed steep strike-slip faults and joints.
 332 Almost all strike-slip faults are arranged in relay segments or in a corridor of segments connected
 333 by extension fractures (Figs. 4a, 4d). Their traces attain 400 m in length in the outcrops, but their
 334 corresponding lineaments mapped in regional-scale DEM hillshade maps reach 80 - 90 km. In
 335 quarries, cross-sectional views of the fault-fracture systems show exposures of up to 50 m in
 336 height.

337 The fold-thrust terrane of the West Congo Belt is composed of two domains with distinct structural
 338 styles. One of the domains is dominated by major NW-trending low- to high-angle thrusts which
 339 control the NE vergence of the belt, and their associated high-angle back-thrusts (Fig. 4b). This
 340 structural style primarily affected schistose rocks with intruded dolerite, diamictites, quartzites,
 341 and sandstones units. The other domain is marked by a basin structure, a synclinorium, that rest
 342 on thrust sheets within the orogenic belt. This basin is dominated by carbonate sequences which
 343 are cut by major NE-trending strike-slip brittle shear zones (Fig. 4e). The strike-slip shear zones
 344 are arranged in step-overs associated with én-echelon extension fractures or normal faults. These
 345 faulting styles are observable down to 200 m depths in the caves of Ngovo and Ndimba. In northern
 346 RC, Archean rocks of Souanké host 2.8 Ga charnokites, gneisses, and pegmatites which are also
 347 deformed by the brittle shear zones. Nearly all the brittle shear zones observed on the field show
 348 linking architecture with relay zones connected either by extension fractures or duplex structures
 349 (Fig. 4c). On a slip surface along the strike-slip faults, we find evidence of over-printing of sub-
 350 horizontal slickenlines by vertical slicklines (Fig. 4f), indicating that these NE-SW, WNW-ESE,
 351 NW-SE and N-S trending strike-slip faults have been reactivated in dip slip.

352

353

354 **Figure 4:** Field observations of faults systems. (a & d) Fault systems in outcrops of the Inkisi Group (Dbk),
 355 showing fracture patterns (highlighted in white dashed line in 3a), and a fault zone showing segmented
 356 faults in a duplex zone (in 3d), at the Kombé quarry, located near the Congo River, Brazzaville. (b & e)
 357 Faults systems (Dwc1 & Dk) in the West-Congo Belt showing successively thrust and back-thrust affecting
 358 schists and quartzites, in Dolisie along the RN1 primary road, and strike-slip fault planes in Kolas quarry
 359 near Loutété region. (c & f) Faults systems (Dso) in Souanké showing high-angle planes of strike-slip faults
 360 in the area (in 3c) and, a NE-trending plane that shows horizontal striae that is over-printed by vertical
 361 striae associated with calcite fibers, indicating a later normal faulting reactivation of the strike-slip faults.
 362 The dashed lines in Fig. 3f represent the directions of striae.

363

364 In addition to the observed brittle deformation along the fault systems, we also note a widespread
 365 occurrence of geochemical alterations along the fault zones. For example, at field sites Dwc1 and
 366 Dk located in the West Congo Belt, several strike-slip fault zones show calcite mineralization that
 367 occur in accretion steps (Figs. 5a-c), and a few other fault zones show iron staining along the fault
 368 planes (Fig. 5b,c,d). Likewise, in the fault zones hosted in schistose terranes (e.g., Dk and Dngov),
 369 we observe networks of quartz veins injected along thrust faults and shear zones (Fig. 5f). In the
 370 sedimentary sequences (Inkisi Group; location Dbk), the fault zones are either mineralized by

371 palygorskite, calcite, or a mix of both (Fig. 5e). However, at all the field sites visited, we commonly
 372 observed brittle reactivation of the mineralized fault and fracture planes evidenced by sheared
 373 mineral fibers with characteristic chatter marks, or tensile fracturing of the mineralized zones.

374
 375

376 **Figure 5:** *Geochemical alterations along mineralized fault surfaces. (a) Accretion calcite steps along NW-*
 377 *SE strike-slip faults in carbonates rocks of the West Congo Belt, DRC. (b - c) Carbonate-hosted faults*
 378 *surfaces covered by accretion calcite steps and iron staining. Note that the carbonate rock in Figure 5b*
 379 *has penetrative cross-bedding structures that should not be confused with slickenlines. (d) Fault surface in*
 380 *Inkisi sandstones associated with iron alteration realm. (e) Slickensided palygorskite along a fault in Dbk*
 381 *fault system. (f) Deformed doleritic intrusion along a high-angle thrust fault (230/40) injected with quartz*
 382 *veins in the Dwcl faults system.*

383

384 **4.3 Contemporary Stress Fields within the Analyzed Sub-Regions**

385 All three sub-regional boxes show a compressional strike-slip (i.e., transpressive) stress regime
 386 with a maximum horizontal compressive stress (SHmax) orientation that lies in the NE-SW
 387 quadrant (Fig. 6). The quality of tensor solutions is of B type, indicating that they are well-
 388 constrained. The standard deviation of the SHmax is less than $\pm 15^\circ$ for all the boxes, as Box 1, 2,
 389 and 3 show SHmax standard deviations of ± 5.7 , ± 11.1 , and ± 14.3 respectively. The nodal planes
 390 of all tensors are in reactivated positions in the Mohr diagram (Figs. 6c, d, f). However, unlike the
 391 Box 2 where SHmax is oriented NE-SW (051° trend, 30° plunge), boxes 1 and 3 are more similar
 392 in that they show an SHmax orientations of NNE-SSW (014° trend, 4° plunge) and N-S (184°
 393 trend, 3° plunge) respectively. In a transpressive stress regime, the SHmax corresponds to the
 394 maximum principal compressive stress (σ_1).

395 Both Boxes 1 and 3 show strike-slip nodal planes that are oriented NW-SE and NE-SW (Figs. 6b,
 396 6b-e); however, Box 1 has events with E-W trending sinistral and high-angle N-S trending normal
 397 nodal planes, and in Box 3, some of the events show conjugate reverse faulting patterns with nodal
 398 planes trending NW-SE and ENE-WSW. In Box 2, most of the nodal planes show high-angle and
 399 low-angle reverse faulting, and some of the high-angle reverse nodal planes show an obliquity
 400 associated with a secondary strike-slip motion. Boxes 1 and 2 yield index R' values of 1.75 and
 401 1.85 (Table 1), indicating that both sub-regions are undergoing a transition between pure strike-
 402 slip and compressional regimes. Whereas, in the continental interior in Box 2, the inversion shows
 403 an index R' of 2.2, suggesting a more dominant compressional regime and less prominent strike-
 404 slip regime.

405

406

407 **Figure 6:** *Results of stress tensors from the inversion of earthquake focal mechanism solution along the*
 408 *western Africa continental margin, offshore and onshore Gulf of Guinea represented by sub-regional boxes*
 409 *(see Fig, 3b).*

410

411

412 **Table 1:** *Stress parameters associated with the focal mechanism solution of earthquakes in Box 1, Box 2,*
 413 *and Box 3 in Figure 2b. n: number of data used, nt: total data, Pl & Az: plunge & azimuth of principal*
 414 *compressive stress tensors, R': index regime; Reg: Regime, QRfm: Quality rank of focal mechanism.*

415

416 **4.4 Slip Tendency of Preexisting Fault systems**

417 The application of stress tensors of Box 1 and Box 2 to the fault systems mapped onshore along
 418 the coastal margin (i.e., Box 1 sub-region) show that several faults that are more likely to be
 419 reactivated if the dominant stress field is that of Box 1 (transpressive with NNE-SSW SHmax;
 420 Figs. 7a,c,e,g & 8a,c,e,g). This sub-region covers the Archean rocks of Souanké, the West Congo
 421 Belt, and approximately the Inkisi Group. The NNW- and NNE-oriented planes of strike-slip faults
 422 showed the highest values of TsN = 80 to 100 %. Also, we note that some of the NNE- and NE-
 423 trending normal faults are in a position of reactivation as they show TsN values of >60 %. Here,
 424 the WNW- to E-W -oriented faults show the lowest values of TsN, suggesting they could not be
 425 reactivated in such stress field. The WNW- to E-W planes are mis-oriented for reactivation as they
 426 plot beneath the failure envelope (residual strength envelope) in the Mohr diagram (see blue circles
 427 in Figs. 7c, d, g, h & 8c, d, g, h). Overall, the Mohr diagram for the Box 1 regime test indicate that
 428 most of the faults are in a position of reactivation.

429 Whereas, assuming the Box 2 stress field (transpressive with NE-SW SHmax; Figs. 7b, f & 8b, d),
 430 very few faults are at failure, suggesting a significantly lower likelihood of reactivation. The
 431 possibility of reactivation of the mapped strike-slip faults and normal faults in the Box 2 stress
 432 regime is less probable as most of the TsN values are <60 %. Only thrust faults in the West Congo
 433 Belt are likely to be reactivated and particularly, the back-thrusts. In Box 2 stress regime, most of
 434 thrust faults show TsN values >60%. However, there are a few thrust faults that are in the position
 435 of reactivation in the Box 1 stress regime; for example, a major thrust fault system that is associated
 436 with the vergence of the orogenic belt (Fig. 8b). Also, in the Box 2 stress regime, the major NE-
 437 oriented planes are fault systems that couldn't be reactivated as they plot beneath the failure
 438 envelope in the Mohr diagram.

439

440 **Figure 7:** *The application of the stress inversion results for Box 1 (left column) and Box 2 (right column)*
 441 *on Dbk and Dso fault systems and the resulting Slip Tendency values associated with their Mohr-Coulomb*
 442 *stress states. The slip tendency estimate associated with each fault segment is presented as color-coded*
 443 *planes in both the stereoplots and their adjoining Mohr diagrams.*

444

445 **Figure 8:** *The application of the stress inversion results for Box 1 (left column) and Box 2 (right column)*
 446 *on Dwc1 and Dwc2 fault systems and the resulting Slip Tendency values associated with the Mohr-Coulomb*
 447 *stress states. The slip tendency estimate associated with each fault segment is presented as color-coded*
 448 *planes in both the stereoplots and their adjoining Mohr diagrams.*

449

450 **5 Discussion**

451 **5.1 The Stress Regime of Earthquakes along the Western Africa Continental Margin**

452 The regional clustering of earthquakes along and in the vicinity of preexisting tectonic lineaments
 453 (Fig. 3a) and the stress tests performed in this study (Figs. 6 - 8) show that earthquakes along the
 454 continental margin of western Africa and western Central Africa are likely associated with
 455 seismogenic reactivation of preexisting fault systems inherited from past tectonic events. These
 456 structures, consist primarily of brittle shear zones developed during the Eburnean orogeny
 457 (Proterozoic), Pan-African Orogeny (Proterozoic), and the opening of the Central and South
 458 Atlantic (Late Cretaceous). The results of stress inversion and stress tests in this study show that

459 most of the actual fault planes would be NW-SW, NNW-SSE, N-S, NNE to NE-SW and less likely
460 E-W trending strike-slip faults/normal faults or NW-SE and E-W trending thrust-faults in Box 1,
461 Box 2 and Box 3 sub-regions. These faults orientations match most of the described fractures
462 systems in the area and in the literature, particularly for Box 3 (Fig.3). In Box 1 and Box 2 sub-
463 regions, the NW- and E-W -oriented thrust faults probably correspond to the orientation of
464 structures within the West-Congo Belt and thrust sheets of the Oubanguides Belt respectively.
465 Both the strike-slip faults and normal faults deform every unit in the sub-regions from Archean
466 through the Cretaceous units. Also, based on the visited field sites with seismic events, the
467 earthquake epicenters are generally located in the vicinity of the large strike-slip fault systems or
468 normal fault zones. For Box 3, strike-slip faults and normal faults would likely correspond to N-S
469 and NNE-trending strike-slip and thrust fault systems of the Dahomeyide Belt (Affaton et al.,
470 1991; Villeneuve & Cornée, 1994) which were later reactivated either in normal faulting or strike-
471 slip faulting.

472 The orientations of nodal planes used in stress inversion determination are consistent with the
473 kinematics of some of the strike-slip, normal, and thrust fault systems with high values of slip
474 tendency in Box 1 and Box 2 stress fields applied to these faults systems in the area (Figs. 6, 7, 8).
475 The NNW-SSE and NNE-SSW features would play as dextral strike-slip faults and sinistral strike-
476 slip faults under the stress regime in Box 1. This situation is satisfied in perfectly in Dso fault
477 system of Souanké (Fig.7e) and with some faults in the Inkisi Group (Fig. 7a). For instance, in the
478 coastal margin, the Monatéle earthquake in Cameroon was associated with a NE-SW trending
479 strike-slip sinistral fault (Ngatchou et al., 2018). This clearly supports the kinematics of actual
480 faults plan acting in this coastal margin. From the coastal margin to inland continent, the results
481 show that there is a partition in stress regime within the western central African continental plate.
482 On the coastal margin a strike-slip faulting regime with a minor compressional regime component
483 prevails, while in the inland, the regime is more compressive with a moderate strike-slip faulting
484 component. This explain why NW-SE to NNE-SE strike-slip faults/normal faults show the most
485 tendency to be reactivated in the costal margin areas during the past or present-day. While for the
486 continental interior areas, the most probable reactivated structures are NW-thrust faults/normal
487 faults systems and less likely strike-slip faults. Delvaux et al. (2017) proposed the development of
488 strike-slip deformation of the Inkisi Group during the opening of the south Atlantic and suggested
489 that the event was associated with the last phase of continental break-up with sub-horizontal
490 maximum compressive stress that is oriented N-S. The inferred stress field of the break-up phase
491 is similar to the stress field calculated for the Box 1 stress-field in this study (Fig.6a). This would
492 indicate that the Box 1 stress field was once acting on the cratonic interior sub-regions but is now
493 restricted to the continental margin areas.

494 Overall, several studies have speculated that preexisting fractures are hosting earthquakes along
495 the continental margins and interior of western Africa but lack details of the ambient stress field
496 and the evidence for coseismic surface fault rupture or presence of active fault scarps (Blundell,
497 1976; Sykes, 1978; Bouka Biona and Sounga, 2001; Bouka Biona and Sounga, 2001; Ayele, 2002;
498 Amponsah, 2002; Kutu, 2013; Olugboji et al., 2021). Here, with our stress analysis, we provide
499 insight into the control of contemporary stress regimes on the occurrence of intraplate earthquakes
500 in the region.

501

502 **5.2 The Inherited Weakness of the Preexisting Fault Systems**

503 Our stress analysis shows that the structural geometries of preexisting fault zone fracture surfaces
504 make them favorably oriented for reactivation in the contemporary stress field. However, although
505 fault orientation and their coefficient of friction in the Mohr-Coulomb space may determine
506 whether a preexisting fault can reactivate, they do not determine whether faults would reactivate
507 by stable creep or by seismic rupture. The susceptibility of faults to seismic or stable creep
508 reactivation is determined by the frictional stability of the faulted rocks at the contemporary
509 temperature and pressure conditions at depth in the crust (Blanpied et al., 1998; Dieterich, 1979;
510 Ikari et al., 2011; Marone, 1998). This phenomenon is true for both active plate boundary settings
511 (e.g., Carpenter et al., 2009) and intraplate settings (e.g., Kolawole et al., 2019).

512 Our field observations of the basement- and sedimentary-hosted fault systems show widespread
513 occurrence of hydrothermal alterations along the fault zones (Fig.5). These hydrothermal
514 alterations include calcite veins, quartz veins, palygorskite gouge fill, a mix of palygorskite and
515 calcite, and iron stains along the fault planes. Also, we note that the fault zones commonly show
516 post-alteration brittle reactivation of the fault zones (e.g., Figs.5b, c, d). The presence of accretion
517 patterns in the calcite realms suggest that there were multiple episodes of hydrothermal incursion
518 into the fault zones. Also, the presence of calcite alterations along fault zones in both the crystalline
519 basement rocks of the West Congo Belt and overlying Inkisi Sandstone units suggest that the large
520 strike-slip fault systems in the sandstone exposures are likely rooted directly into the basement and
521 both structural levels have shared at least one episode of hydrothermal circulation in the past.
522 However, more importantly, the most-common alteration minerals along the fault zones, calcite
523 and palygorskite, are known from laboratory experiments to show frictional instability ($0 > a-b >$
524 -0.013) at temperature and pressure conditions relevant to a seismogenic depth interval in the upper
525 crust (Kolawole et al., 2019; Sánchez-Roa et al., 2017; Verberne et al., 2015).

526 Overall, the fault zones investigated in the field are generally dry in present-day. Also, besides from
527 the Cameroon Volcanic Line and the Angolan Bié Dome, hot springs are very rare and there is no
528 large-scale geothermal high-anomaly along the western Africa onshore continental margin areas
529 (Macgregor, 2020; Waring et al., 1965). The occurrence of hot springs in both the Cameroon
530 Volcanic Line and Bié Dome are understandable since both are known zones of localized mantle
531 upwelling (Reusch et al., 2010; Walker et al., 2016). The sparseness of hot springs in the region
532 suggests that seismic reactivation of the intraplate fault zones is not likely driven by crustal
533 circulation of hot fluids. Therefore, considering the widespread occurrence of minerals like calcite,
534 quartz, and palygorskite along the fault zones, we suggest that the seismic stability conditions of
535 the faulted rocks at depth may be contributing to the susceptibility of the onshore fault zones to
536 seismic reactivation.

537

538 **5.3 Possible Origins of Stress Loading along the Western Africa Continental Margin**

539 Again, aside from the Cameroon Volcanic Line and Bié Dome in Angola, where active mantle
540 processes are driving magmatic activities and associated earthquakes (De Plaen et al., 2014; Tabod
541 et al., 1992; Ubangoh et al., 1997), the origin of stress loading leading to seismogenic rupture of
542 preexisting faults in the onshore areas of the western Africa's continental margin remains
543 controversial and less understood (Olugboji et al., 2021). The proposed mechanisms include the
544 reactivation of local basement fractures by far-field tectonic stresses from mantle processes along
545 the Cameroon volcanic line, post-rift crustal relaxation along the rifted margin, landward
546 continuation of oceanic fracture zones, and induced earthquakes triggered by groundwater
547 extraction (Olugboji et al., 2021).

548 The zone of earthquake clustering along the Ghanaian coastal margin, shown in Fig. 3a, is
549 collocated with NNE-trending Quaternary faults (Akwapim, Lokossa, and Séhoué Faults) which
550 splay northwards from the northeastern tip zone of the Chain Fracture Zone offshore, defining a
551 Reidel horsetail-pattern geometry within the fracture zone (Burke, 1969). However, (Burke, 1969)
552 rightfully noted that there is no evidence of continuity of fault trace further inland from this region.
553 However, just east of the Ghana region, brittle deformation of basement massifs further inland in
554 SW Nigeria show the pervasive presence of satellite-scale ENE-trending fracture systems
555 (Anifowose & Kolawole, 2012) that trend parallel to the near-shore segments of the oceanic
556 fracture zones. Likewise, in this study, onshore large-scale lineament mapping and detailed field
557 mapping of fault systems show the presence of ENE-to-NE-trending fault systems that do not
558 extend directly offshore, but also trend parallel to the near-shore segments of the oceanic fracture
559 zones (Figs. 1, 3a). It was also proposed that channeling of melt along the northeastward extension
560 of the Ascension Fracture Zone across the continent-ocean boundary and further onshore
561 influenced the development of the Cameroon Volcanic Line (Reusch et al., 2010). However, the
562 NE-SW oriented extensional structures would have formed parallel to the shortening axis and
563 approximately to the maximum compressive stress (Woodcock & Schubert, 1994).
564 In addition to the observation of similar structural trends between oceanic fracture zones and
565 onshore fault and fracture systems, our analysis shows that the stresses acting on the offshore
566 oceanic fracture zones are comparable with the stresses acting along the onshore areas of the
567 continental margin (Figs. 6a-b and 6e); and that the onshore fault systems have a high slip tendency
568 in this contemporary stress field (Figs. 7-8). Given that the oceanic fracture zones are active
569 intraplate faults possibly activated by far-field strain transfer from transform faults along the
570 spreading ridges (Fig. 2a; Meghraoui et al., 2019), we propose that northeastward stress
571 propagation into the near-shore and onshore tip zones of the oceanic fracture zones may be driving
572 stress loading on pre-stressed fault systems onshore, leading to fault reactivation in the onshore
573 areas.

574

575 **6 Conclusions**

576 In this study, we compute the contemporary stress field along the coastal margin of western Africa
577 and some of the interior cratonic areas, map pre-existing fault systems in basement and
578 sedimentary outcrops along the margin, and assess the reactivation potential of the mapped
579 structural planes. Our results show that:

- 580 • Intraplate earthquakes along the continental margin of West Africa and western Central
581 Africa cluster along or in the vicinity of preexisting brittle shear zones and thrust faults,
582 suggesting a potential for brittle reactivation of preexisting structures.
- 583 • The earthquakes originate under a transpressive stress regime with the maximum principal
584 compressive stress (σ_1 , parallel to SHmax) oriented NNE-SSW.
- 585 • In this contemporary stress field, the pre-existing NNE-, NNW-, and N-S -trending strike-
586 slip faults and normal faults show a high slip tendency (60 – 100 %), suggesting a high
587 likelihood to be reactivated. Whereas in the cratonic interior of western Central Africa, the
588 NW- and N-S -trending thrust faults are the most probable structures to be reactivated.
- 589 • In both the basement and sedimentary cover rocks, paleo- hydrothermal alterations of the
590 fault zones are common. Although, in present-day, the fault zones are generally dry, the

591 high likelihood of reactivation (based on our stress tests) and presence of fault rock
 592 frictionally unstable materials on fault planes (minerals like palygorskite and calcite)
 593 suggest that the faults may be susceptible to frictional instability and earthquake nucleation
 594 during their reactivation.

595 • Our stress analysis show that the regional stresses acting on offshore oceanic fracture zones
 596 are compatible with the stresses acting along the onshore areas of the continental margin;
 597 and that the onshore pre-existing strike-slip faults, which are parallel to the oceanic fracture
 598 zones, have a high slip tendency in this contemporary stress field.

599 • We propose that northeastward stress propagation into the near-shore and onshore tip zones
 600 of the oceanic fracture zones may be driving stress loading on pre-stressed fault systems
 601 onshore, leading to fault reactivation in the onshore areas.

602

603 *Acknowledgments*

604 The authors declare that they have no known competing financial interests or personal
 605 relationships that could have appeared to influence the work reported in this paper. This work is
 606 part of the PhD thesis of Nkodia Hardy. It is funded by Coopération Belge and ACCORDCAD,
 607 under the GEORES4DEV program, for his PhD through the support of the Royal Museum of
 608 Central Africa. We thank the reviewers for their great help to improve this manuscript. We also
 609 thank Mr. Elvis Kongota and Prof. Valentin Kanda Nkula for their administrative help in
 610 Democratic Republic of Congo.

611 *Data Availability Statement*

612 The earthquake data used in this study can be downloaded in the International Seismic Center
 613 (ISC), the United States Geological Survey (USGS), the Global Centroid-Moment-Tensor (CMT),
 614 and the GFZ GEOFON earthquake catalogs. The focal mechanism data and field measurements
 615 that support the analysis in this study are provided in the supplementary documents of the
 616 manuscript. The version 5.9.1 of the Win-Tensor free-access software was used to determine stress
 617 from focal mechanism and for the assessment of fault slip tendency. The software can be
 618 downloaded from <http://damiendelvaux.be/Tensor/tensor-index.html> (D. Delvaux, 2012).

619

620 **Credit Author statement**

621 **DVMHN:** Conceptualization, Methodology, Data Curation, Investigation, Writing-Original;
 622 Writing- review & editing; Visualization, Formal analysis, Project administration; **TM:**
 623 Conceptualization; Methodology, Investigation; Reviewing; **FK:** Methodology, Writing- review
 624 & editing, Visualization, Validation; **FB:** Conceptualization, Investigation, Supervision, Project
 625 administration, Funding Acquisition, Reviewing; **APRL:** Investigation; reviewing; **NCBT:**
 626 Investigation and reviewing; **DD:** Methodology, Writing- review & editing, Supervision,
 627 Investigation; Validation; Resources, Data Curation, Funding Acquisition.

628 *References*

629 Adepelumi, A. A., Ako, B. D., Ajayi, T. R., Olorunfemi, A. O., Awoyemi, M. O., & Falebita, D. E. (2008).
 630 Integrated geophysical mapping of the Ifewara transcurrent fault system, Nigeria. *Journal of African Earth*
 631 *Sciences*, 52(4), 161–166. <https://doi.org/10.1016/j.jafrearsci.2008.07.002>

- 632 Affaton, P., Rahaman, M. A., Trompette, R., & Sougy, J. (1991). The Dahomeyide Orogen: tectonothermal
 633 evolution and relationships with the Volta Basin. In *The West African orogens and circum-Atlantic*
 634 *correlatives* (pp. 107–122). Springer.
- 635 Ajakaiye, D., Hall, D., Millar, T., Verheijen, P., Awad, M., & Ojo, S. (1986). Aeromagnetic anomalies and tectonic
 636 trends in and around the Benue Trough, Nigeria. *Nature*, *319*, 582–584. <https://doi.org/10.1038/319582a0>
- 637 Akame, J. M., Owona, S., Hublet, G., & Debaille, V. (2020). Archean tectonics in the sangmelima granite-
 638 greenstone terrains, Ntem Complex (NW Congo craton), southern Cameroon. *Journal of African Earth*
 639 *Sciences*, *168*, 103872. <https://doi.org/10.1016/j.jafrearsci.2020.103872>
- 640 Akame, J. M., Schulz, B., Owona, S., & Debaille, V. (2021). Monazite EPMA-CHIME dating of Sangmelima
 641 granulite and granitoid rocks in the Ntem Complex, Cameroon: Implications for Archean tectono-thermal
 642 evolution of NW Congo craton. *Journal of African Earth Sciences*, *181*, 104268.
 643 <https://doi.org/10.1016/j.jafrearsci.2021.104268>
- 644 Alvarez, P., & Maurin, J.-C. (1991). Evolution sédimentaire et tectonique du bassin protdrozoïque supérieur de
 645 Comba (Congo): stratigraphie séquentielle du Supergroupe Ouest-Congolien et modèle d’amortissement
 646 sur décrochements dans le contexte de la tectogénèse panafricaine, *50*, 137–171.
- 647 Ambraseys, N. N., & Adams, R. D. (1986). Seismicity of West Africa. *Seismicity of West Africa*, *4*(6), 679–702.
- 648 Amponsah, P., Leydecker, G., & Muff, R. (2012). Earthquake catalogue of Ghana for the time period 1615–2003
 649 with special reference to the tectono-structural evolution of south-east Ghana. *Journal of African Earth*
 650 *Sciences*, *75*, 1–13. <https://doi.org/10.1016/j.jafrearsci.2012.07.002>
- 651 Amponsah, P. E. (2002). Seismic activity in relation to fault systems in southern Ghana. *Journal of African Earth*
 652 *Sciences*, *35*(2), 227–234. [https://doi.org/10.1016/S0899-5362\(02\)00100-8](https://doi.org/10.1016/S0899-5362(02)00100-8)
- 653 Angelier, J. (1975). Sur l’analyse de mesures recueillies dans des sites faillés: l’utilité d’une confrontation entre les
 654 méthodes dynamiques et cinématiques: erratum. *Comptes-Rendus de l’Académie Des Sciences*, *283*, 466.
- 655 Angelier, J. (1989). From orientation to magnitudes in paleostress determinations using fault slip data. *Journal of*
 656 *structural geology*, *11*(1/2), 37–50.
- 657 Angelier, J., & Mechler, P. (1977). Sur une methode graphique de recherche des contraintes principales egalement
 658 utilisables en tectonique et en seismologie : la methode des diedres droits. *Bulletin de La Société*
 659 *Géologique de France*, *S7-XIX*(6), 1309–1318. <https://doi.org/10.2113/gssgfbull.S7-XIX.6.1309>
- 660 Anifowose, A. Y. B., & Kolawole, F. (2012). Emplacement Tectonics of Idanre Batholith, West Africa.
 661 *Comunicação Geológicas*, *99*(2).
- 662 Antobreh, A. A., Faleide, J. I., Tsikalas, F., & Planke, S. (2009). Rift–shear architecture and tectonic development of
 663 the Ghana margin deduced from multichannel seismic reflection and potential field data. *Marine and*
 664 *Petroleum Geology*, *26*(3), 345–368. <https://doi.org/10.1016/j.marpetgeo.2008.04.005>
- 665 Assumpção, M. (1998). Seismicity and stresses in the Brazilian passive margin. *Bulletin of the Seismological Society*
 666 *of America*, *88*(1), 160–169.
- 667 Awoyemi, M., & Onyedim, G. (2004). Relationship between air photo lineament and fracture patterns of Ilesha,
 668 southwestern Nigeria. *African Geoscience Review*, *11*(1), 81–90.
- 669 Awoyemi, M. O., Hammed, O. S., Falade, S. C., Arogundade, A. B., Ajama, O. D., Iwalehin, P. O., & Olurin, O. T.
 670 (2017). Geophysical investigation of the possible extension of Ifewara fault zone beyond Ilesa area,
 671 southwestern Nigeria. *Arabian Journal of Geosciences*, *10*(2), 27. [https://doi.org/10.1007/s12517-016-](https://doi.org/10.1007/s12517-016-2813-z)
 672 [2813-z](https://doi.org/10.1007/s12517-016-2813-z)
- 673 Batumike, M. J., Kampunzu, A. B., & Cailteux, J. H. (2006). Petrology and geochemistry of the Neoproterozoic
 674 Nguba and Kundelungu Groups, Katangan Supergroup, southeast Congo: implications for provenance,
 675 paleoweathering and geotectonic setting. *Journal of African Earth Sciences*, *44*(1), 97–115.
- 676 Benkhelil, J. (1989). The origin and evolution of the Cretaceous Benue Trough (Nigeria). *Journal of African Earth*
 677 *Sciences (and the Middle East)*, *8*(2–4), 251–282.
- 678 Blanpied, M. L., Tullis, T. E., & Weeks, J. D. (1998). Effects of slip, slip rate, and shear heating on the friction of
 679 granite. *Journal of Geophysical Research: Solid Earth*, *103*(B1), 489–511.
 680 <https://doi.org/10.1029/97JB02480>
- 681 Blundell, D. J. (1976). Active faults in West Africa. *Earth and Planetary Science Letters*, *31*(2), 287–290.
 682 [https://doi.org/10.1016/0012-821X\(76\)90221-1](https://doi.org/10.1016/0012-821X(76)90221-1)
- 683 Boudzoumou, F., & Trompette, R. (1988). La chaîne panafricaine ouest-congolienne au Congo (Afrique
 684 équatoriale); un socle polycyclique charrie sur un domaine subautochtone forme par l’aulacogene du
 685 Mayombe et le bassin de l’Ouest-Congo. *Bulletin de La Société Géologique de France*, *4*(6), 889–896.

- 686 Bouenitela, T. T. V. (2019). *LE DOMAINE PALEOPROTEROZOIQUE (EBURNEEN) DE LA CHAINE DU*
687 *MAYOMBE (CONGO-BRAZZAVILLE) : origine et évolution tectono-métamorphique*. Université de
688 Rennes 1, Rennes.
- 689 Bouka Biona, C., & Sounga, J.-D. (2001). Corrélation entre la localisation des foyers des séismes et les zones de
690 délimitation des horsts et des grabens su soubassement de la Cuvette Congolaise (Afrique Centrale).
691 *Annales Université Brazzaville*, 2(1), 125–139.
- 692 Burbank, D. W., & Anderson, R. S. (2011). *Tectonic Geomorphology*. John Wiley & Sons.
- 693 Burke, K. (1969). Seismic Areas of the Guinea Coast where Atlantic Fracture Zones reach Africa. *Nature*,
694 222(5194), 655–657. <https://doi.org/10.1038/222655b0>
- 695 Calais, E., Camelbeeck, T., Stein, S., Liu, M., & Craig, T. J. (2016). A new paradigm for large earthquakes in stable
696 continental plate interiors. *Geophysical Research Letters*, 43(20), 10,621–10,637.
697 <https://doi.org/10.1002/2016GL070815>
- 698 Carpenter, B. M., Marone, C., & Saffer, D. M. (2009). Frictional behavior of materials in the 3D SAFOD volume.
699 *Geophysical Research Letters*, 36(5). <https://doi.org/10.1029/2008GL036660>
- 700 De Carvalho, H., Tassinari, C., Alves, P. H., Guimarães, F., & Simões, M. C. (2000). Geochronological review of
701 the Precambrian in western Angola: links with Brazil. *Journal of African Earth Sciences*, 31(2), 383–402.
702 [https://doi.org/10.1016/S0899-5362\(00\)00095-6](https://doi.org/10.1016/S0899-5362(00)00095-6)
- 703 De Long, S. E., Dewey, J. F., & Fox, P. J. (1977). Displacement history of oceanic fracture zones. *Geology*, 5(4),
704 199–202. [https://doi.org/10.1130/0091-7613\(1977\)5<199:DHOOFZ>2.0.CO;2](https://doi.org/10.1130/0091-7613(1977)5<199:DHOOFZ>2.0.CO;2)
- 705 De Plaen, R. S. M., Bastow, I. D., Chambers, E. L., Keir, D., Gallacher, R. J., & Keane, J. (2014). The development
706 of magmatism along the Cameroon Volcanic Line: Evidence from seismicity and seismic anisotropy.
707 *Journal of Geophysical Research: Solid Earth*, 119(5), 4233–4252. <https://doi.org/10.1002/2013JB010583>
- 708 Delteil, J.-R., Valery, P., Montadert, L., Fondeur, C., Patriat, P., & Mascle, J. (1974). Continental Margin in the
709 Northern Part of the Gulf of Guinea. In C. A. Burk & C. L. Drake (Eds.), *The Geology of Continental*
710 *Margins* (pp. 297–311). Berlin, Heidelberg: Springer. https://doi.org/10.1007/978-3-662-01141-6_22
- 711 Delvaux, D. (2012). Release of program Win-Tensor 4.0 for tectonic stress inversion: statistical expression of stress
712 parameters. In *Geophysical research abstracts* (Vol. 14). EGU General Assembly Vienna.
- 713 Delvaux, Damien, & Bath. (2010). African stress pattern from formal inversion of focal mechanism data.
714 *Tectonophysics*, 482, 105–128.
- 715 Delvaux, Damien, Everaerts, M., Kongota Isasi, E., & Ganza Bamulezi, G. (2016). Intraplate compressional
716 deformation in West-Congo and the Congo basin: related to ridge-puch from the South Atlantic spreading
717 ridge? In *EGU General Assembly Conference Abstracts* (Vol. 18).
- 718 Delvaux, Damien, Ganza, G., Kongota, E., Fukiabantu, G., Mbokola, D., Boudzoumou, F., et al. (2017). The " fault
719 of the Pool" along the Congo River between Kinshasa and Brazzaville, R (D) Congo is no more a myth:
720 Paleostress from small-scale brittle structures. In *EGU General Assembly Conference Abstracts* (Vol. 19, p.
721 15143).
- 722 Delvaux, Damien, Maddaloni, F., Tesauro, M., & Braitenberg, C. (2021). The Congo Basin: Stratigraphy and
723 subsurface structure defined by regional seismic reflection, refraction and well data. *Global and Planetary*
724 *Change*, 198, 103407. <https://doi.org/10.1016/j.gloplacha.2020.103407>
- 725 Dieterich, J. H. (1979). Modeling of rock friction: 1. Experimental results and constitutive equations. *Journal of*
726 *Geophysical Research: Solid Earth*, 84(B5), 2161–2168. <https://doi.org/10.1029/JB084iB05p02161>
- 727 Fail, J. P., Montadert, L., Delteil, J. R., Valery, P., Patriat, Ph., & Schlich, R. (1970). Prolongation des zones de
728 fractures de l'océan atlantique dans le golfe de guinee. *Earth and Planetary Science Letters*, 7(5), 413–419.
729 [https://doi.org/10.1016/0012-821X\(70\)90083-X](https://doi.org/10.1016/0012-821X(70)90083-X)
- 730 Fullgraf, T., Callec, Y., Thiéblemont, D., Gloaguen, E., Charles, N., Métour, J., et al. (2015). *Notice explicative de*
731 *la carte géologique de la République du Congo à 1/200 000, Feuille Dolisie*. (F). République du Congo:
732 Editions BRGM.
- 733 Gatsé Ebotenhouna, C., Xie, Y., Adomako-Ansah, K., Gourcerol, B., & Qu, Y. (2021). Depositional Environment
734 and Genesis of the Nabeba Banded Iron Formation (BIF) in the Ivindo Basement Complex, Republic of the
735 Congo: Perspective from Whole-Rock and Magnetite Geochemistry. *Minerals*, 11(6), 579.
736 <https://doi.org/10.3390/min11060579>
- 737 GEBCO Bathymetric Compilation Group 2021. (2021). The GEBCO_2021 Grid - a continuous terrain model of the
738 global oceans and land. *NERC EDS British Oceanographic Data Centre NOC*.
739 <https://doi.org/doi:10.5285/c6612cbe-50b3-0cff-e053-6c86abc09f8f>
- 740 Gerya, T. (2012). Origin and models of oceanic transform faults. *Tectonophysics*, 522–523, 34–54.
741 <https://doi.org/10.1016/j.tecto.2011.07.006>

- 742 Gorini, M. A., & Bryan, G. (1976). The tectonic fabric of the equatorial Atlantic and adjoining continental margins:
 743 Gulf of Guinea to the northeastern Brazil. (Vol. 48, pp. 101–119). Presented at the An. Acad. Brasil.
 744 Cienc., Sao Paulo.
- 745 Grigoli, F., Cesca, S., Priolo, E., Rinaldi, A. P., Clinton, J. F., Stabile, T. A., et al. (2017). Current challenges in
 746 monitoring, discrimination, and management of induced seismicity related to underground industrial
 747 activities: A European perspective. *Reviews of Geophysics*, 55(2), 310–340.
- 748 Guiraud, M., Buta-Neto, A., & Quesne, D. (2010). Segmentation and differential post-rift uplift at the Angola
 749 margin as recorded by the transform-rifted Benguela and oblique-to-orthogonal-rifted Kwanza basins.
 750 *Marine and Petroleum Geology*, 27(5), 1040–1068. <https://doi.org/10.1016/j.marpetgeo.2010.01.017>
- 751 Gupta, H. K., Rastogi, B. K., Mohan, I., Rao, C. V. R. K., Sarma, S. V. S., & Rao, R. U. M. (1998). An investigation
 752 into the Latur earthquake of September 29, 1993 in southern India. *Tectonophysics*, 287(1), 299–318.
 753 [https://doi.org/10.1016/S0040-1951\(98\)80075-9](https://doi.org/10.1016/S0040-1951(98)80075-9)
- 754 Heezen, B. C., Bunce, E. T., Hersey, J. B., & Tharp, M. (1964). Chain and romanche fracture zones. *Deep Sea*
 755 *Research and Oceanographic Abstracts*, 11(1), 11–33. [https://doi.org/10.1016/0011-7471\(64\)91079-4](https://doi.org/10.1016/0011-7471(64)91079-4)
- 756 Heezen, B. C., Tharp, M., Blackett, P. M. S., Bullard, E., & Runcorn, S. K. (1965). Tectonic fabric of the Atlantic
 757 and Indian oceans and continental drift. *Philosophical Transactions of the Royal Society of London. Series*
 758 *A, Mathematical and Physical Sciences*, 258(1088), 90–106. <https://doi.org/10.1098/rsta.1965.0024>
- 759 Hensen, C., Duarte, J. C., Vannucchi, P., Mazzini, A., Lever, M. A., Terrinha, P., et al. (2019). Marine Transform
 760 Faults and Fracture Zones: A Joint Perspective Integrating Seismicity, Fluid Flow and Life. *Frontiers in*
 761 *Earth Science*, 7, 39. <https://doi.org/10.3389/feart.2019.00039>
- 762 Holford, S. P., Hillis, R. R., Hand, M., & Sandiford, M. (2011). Thermal weakening localizes intraplate deformation
 763 along the southern Australian continental margin. *Earth and Planetary Science Letters*, 305(1), 207–214.
 764 <https://doi.org/10.1016/j.epsl.2011.02.056>
- 765 Hossié, G. (1980). *Contribution à l'étude structurale de la chaîne ouest-congolienne(pan-africaine) dans le*
 766 *Mayombe congolais*. (Thesis). University of Montpellier, Montpellier.
- 767 Ikari, M. J., Marone, C., & Saffer, D. M. (2011). On the relation between fault strength and frictional stability.
 768 *Geology*, 39(1), 83–86. <https://doi.org/10.1130/G31416.1>
- 769 Jelsma, H. A., McCourt, S., Perritt, S. H., & Armstrong, R. A. (2018). The Geology and Evolution of the Angolan
 770 Shield, Congo Craton. In S. Siegesmund, M. A. S. Basei, P. Oyhantçabal, & S. Oriolo (Eds.), *Geology of*
 771 *Southwest Gondwana* (pp. 217–239). Cham: Springer International Publishing. [https://doi.org/10.1007/978-](https://doi.org/10.1007/978-3-319-68920-3_9)
 772 [3-319-68920-3_9](https://doi.org/10.1007/978-3-319-68920-3_9)
- 773 Junner, N. R., & Bates, D. A. (1941). *The accra earthquake of 22nd June, 1939*. FJ Miller.
- 774 Kadima, E., Delvaux, D., Sebagenzi, S. N., Tack, L., & Kabeya, S. M. (2011). Structure and geological history of
 775 the Congo Basin: an integrated interpretation of gravity, magnetic and reflection seismic data. *Basin*
 776 *Research*, 23(5), 499–527.
- 777 Kadiri, A. U., & Kijko, A. (2021). Seismicity and seismic hazard assessment in West Africa. *Journal of African*
 778 *Earth Sciences*, 183, 104305. <https://doi.org/10.1016/j.jafrearsci.2021.104305>
- 779 Keranen, K. M., & Weingarten, M. (2018). Induced Seismicity. *Annual Review of Earth and Planetary Sciences*,
 780 46(1), 149–174. <https://doi.org/10.1146/annurev-earth-082517-010054>
- 781 Kessi, C. (1992). *Le socle Archéen et les formations ferrifères du Chaillu au Congo* (Thèse Doctorat). Université de
 782 Rennes 1, Rennes.
- 783 Kolawole, F., Johnston, C. S., Morgan, C. B., Chang, J. C., Marfurt, K. J., Lockner, D. A., et al. (2019). The
 784 susceptibility of Oklahoma's basement to seismic reactivation. *Nature Geoscience*, 12(10), 839–844.
 785 <https://doi.org/10.1038/s41561-019-0440-5>
- 786 Kolawole, Folarin, Atekwana, E. A., Malloy, S., Stamps, D. S., Grandin, R., Abdelsalam, M. G., et al. (2017).
 787 Aeromagnetic, gravity, and Differential Interferometric Synthetic Aperture Radar analyses reveal the
 788 causative fault of the 3 April 2017 Mw 6.5 Moiyabana, Botswana, earthquake. *Geophysical Research*
 789 *Letters*, 44(17), 8837–8846.
- 790 Krenkel, E. (1923). Die Seismizität Afrikas. *Zentralbl. Mineral. Geol. Palaeontol*, 6, 173–183.
- 791 Kutu, J. M. (2013). Seismic and Tectonic Correspondence of Major Earthquake Regions in Southern Ghana with
 792 Mid-Atlantic Transform-Fracture Zones. *International Journal of Geosciences*, 2013.
 793 <https://doi.org/10.4236/ijg.2013.410128>
- 794 Lay, T. (2019). Chapter 4 - Reactivation of Oceanic Fracture Zones in Large Intraplate Earthquakes? In J. C. Duarte
 795 (Ed.), *Transform Plate Boundaries and Fracture Zones* (pp. 89–104). Elsevier.
 796 <https://doi.org/10.1016/B978-0-12-812064-4.00004-9>

- 797 Levandowski, W., Zellman, M., & Briggs, R. (2017). Gravitational body forces focus North American intraplate
798 earthquakes. *Nature Communications*, 8(1), 1–9.
- 799 Lisle, R. J., & Srivastava, D. C. (2004). Test of the frictional reactivation theory for faults and validity of fault-slip
800 analysis. *Geology*, 32(7), 569. <https://doi.org/10.1130/G20408.1>
- 801 Loemba, A. P. A., Nkodia, H. M. D.-V., Bazebizonza Tchiguina, N. C., Miyouna, T., & Boudzoumou, F. (2022).
802 Tectonic and structural evolution of major shear zone in the Ntem-Chaillu Block, in the Ivindo region, in
803 Republic of Congo (p. 53). Presented at the Tectonic Studies Group 2022, Online.
- 804 Lund Snee, J.-E., & Zoback, M. D. (2020). Multiscale variations of the crustal stress field throughout North
805 America. *Nature Communications*, 11(1), 1951. <https://doi.org/10.1038/s41467-020-15841-5>
- 806 Macgregor, D. S. (2020). Regional variations in geothermal gradient and heat flow across the African plate. *Journal*
807 *of African Earth Sciences*, 171, 103950. <https://doi.org/10.1016/j.jafrearsci.2020.103950>
- 808 Marone, C. (1998). Laboratory-Derived Friction Laws and Their Application to Seismic Faulting. *Annual Review of*
809 *Earth and Planetary Sciences*, 26(1), 643–696. <https://doi.org/10.1146/annurev.earth.26.1.643>
- 810 Mascle, J., & Sibuet, J.-C. (1974). New pole for early opening of South Atlantic. *Nature*, 252(5483), 464–465.
- 811 Mbéri Kongo, M. T. G. (2018). *Tectonique de la série des plateaux Batékés dans la zone de Inoni et d'Ekoti ya*
812 *MonSeigneur, République du Congo* (Master thesis). Marien Ngouabi, Brazzaville.
813 <https://doi.org/10.13140/RG.2.2.14583.34729>
- 814 McCaffrey, R. (2008). Global frequency of magnitude 9 earthquakes. *Geology*, 36(3), 263–266.
815 <https://doi.org/10.1130/G24402A.1>
- 816 Meghraoui, M., Amponsah, P., Bernard, P., & Ateba, B. (2019). Active transform faults in the Gulf of Guinea:
817 insights from geophysical data and implications for seismic hazard assessment. *Canadian Journal of Earth*
818 *Sciences*, 56(12), 1398–1408. <https://doi.org/10.1139/cjes-2018-0321>
- 819 Milesi, J. P., Frizon de Lamotte, D., de Kock, G., & Toteu, F. (2010). Tectonic map of Africa (2nd edition).
- 820 Miranda, T., S., Neves, S., P., Celstino, M.-A., L., & Roberts, N., M. W. (2020). Structural evolution of the Cruzeiro
821 do Nordeste shear zone (NE Brazil): Brasiliano-Pan-African- ductile-to-brittle transition and Cretaceous
822 brittle reactivation. *Journal of Structural Geology*, 141, 1–17.
- 823 Miyouna, T., Dieu-Veill Nkodia, H. M., Essouli, O. F., Dabo, M., Boudzoumou, F., & Delvaux, D. (2018). Strike-
824 slip deformation in the Inkisi Formation, Brazzaville, Republic of Congo. *Cogent Geoscience*, 4(1),
825 1542762.
- 826 Morris, A., Ferrill, D. A., & Henderson, D. B. (1996). Slip-tendency analysis and fault reactivation. *Geology*, 24(3),
827 275–278. [https://doi.org/10.1130/0091-7613\(1996\)024<0275:STAAFR>2.3.CO;2](https://doi.org/10.1130/0091-7613(1996)024<0275:STAAFR>2.3.CO;2)
- 828 Moulin, M., Aslanian, D., & Unternehr, P. (2010). A new starting point for the South and Equatorial Atlantic Ocean.
829 *Earth-Science Reviews*, 98(1–2), 1–37.
- 830 Musson, R. M. W. (1992). The seismicity of West and Central Africa. In S. J. Freeth, C. O. Ofoegbu, & K. M.
831 Onuoha (Eds.), *Natural Hazards in West and Central Africa* (pp. 7–11). Wiesbaden: Vieweg+Teubner
832 Verlag. https://doi.org/10.1007/978-3-663-05239-5_2
- 833 Ngako, V., Affaton, P., Nnange, J. M., & Njanko, T. (2003). Pan-African tectonic evolution in central and southern
834 Cameroon: transpression and transtension during sinistral shear movements. *Journal of African Earth*
835 *Sciences*, 36(3), 207–214.
- 836 Ngako, Vincent, Jegouzo, P., & Nzenti, J.-P. (1991). Le cisaillement centre camerounais. Rôle structural et
837 géodynamique dans l'orogénèse panafricaine. *Le Cisaillement Centre Camerounais. Rôle Structural et*
838 *Géodynamique Dans l'orogénèse Panafricaine*, 313(4), 457–463.
- 839 Ngatchou, H. E., Nguiya, S., Owona Angue, M., Mouzong, P. M., & Tokam, A. P. (2018). Source characterization
840 and tectonic implications of the M4.6 Monatélé (Cameroon) earthquake of 19 March 2005. *Geological*
841 *Society of South Africa*.
- 842 Njonfang, E., Ngako, V., Moreau, C., Affaton, P., & Diot, H. (2008). Restraining bends in high temperature shear
843 zones: the “Central Cameroon Shear Zone”, Central Africa. *Journal of African Earth Sciences*, 52(1–2), 9–
844 20.
- 845 Nkodia, H. M. D.-V., Miyouna, T., Delvaux, D., & Boudzoumou, F. (2020). Flower structures in sandstones of the
846 Paleozoic Inkisi Group (Brazzaville, Republic of Congo): evidence for two major strike-slip fault systems
847 and geodynamic implications. *South African Journal of Geology*, 123(4), 531–550.
848 <https://doi.org/10.25131/sajg.123.0038>
- 849 Nkodia, Hardy Medry Dieu-Veill, Boudzoumou, F., Miyouna, T., Ibarra-Gnianga, A., & Delvaux, D. (2021). A
850 progressive episode of deformation in the foreland of the WestCongo Belt: From folding to brittle shearing,
851 in Republic of Congo (p. 1). Presented at the European Gesociences Union, online.

- 852 Nwankwoala, H., & Orji, O. (2018). An Overview of Earthquakes and Tremors in Nigeria: Occurrences,
853 Distributions and Implications for Monitoring. *International Journal of Geology and Earth Sciences*, 4, 56.
854 <https://doi.org/10.32937/IJGES.4.4.2018.56-76>
- 855 Ofoegbu, C. O. (1985). A review of the geology of the Benue Trough, Nigeria. *Journal of African Earth Sciences*
856 (1983), 3(3), 283–291. [https://doi.org/10.1016/0899-5362\(85\)90001-6](https://doi.org/10.1016/0899-5362(85)90001-6)
- 857 Oha, I. A., Okonkwo, I. A., & Dada, S. S. (2020). Wrench tectonism and intracontinental basin sedimentation: a
858 case study of the moku sub-basin, upper benue trough, Nigeria. *J. Geogr. Geol.*, 12(1), 65–75.
- 859 Okal, E. A., & Stewart, L. M. (1982). Slow earthquakes along oceanic fracture zones: evidence for asthenospheric
860 flow away from hotspots? *Earth and Planetary Science Letters*, 57(1), 75–87. [https://doi.org/10.1016/0012-821X\(82\)90174-1](https://doi.org/10.1016/0012-821X(82)90174-1)
- 862 Oladejo, O. P., Adagunodo, T. A., Sunmonu, L. A., Adabanija, M. A., Enemuwe, C. A., & Isibor, P. O. (2020).
863 Aeromagnetic mapping of fault architecture along Lagos–Ore axis, southwestern Nigeria. *Open*
864 *Geosciences*, 12(1), 376–389. <https://doi.org/10.1515/geo-2020-0100>
- 865 Olugboji, T. M., Shirzaei, M., Lu, Y., Adepelumi, A. A., & Kolawole, F. (2021). On the Origin of Orphan Tremors
866 & Intraplate Seismicity in Western Africa. *Earth and Space Science Open Archive ESSOAr*.
- 867 Reusch, A. M., Nyblade, A. A., Wiens, D. A., Shore, P. J., Ateba, B., Tabod, C. T., & Nnange, J. M. (2010). Upper
868 mantle structure beneath Cameroon from body wave tomography and the origin of the Cameroon Volcanic
869 Line. *Geochemistry, Geophysics, Geosystems*, 11(10). <https://doi.org/10.1029/2010GC003200>
- 870 Sánchez-Roa, C., Faulkner, D. R., Boulton, C., Jimenez-Millan, J., & Nieto, F. (2017). How phyllosilicate mineral
871 structure affects fault strength in Mg-rich fault systems. *Geophysical Research Letters*, 44(11), 5457–5467.
872 <https://doi.org/10.1002/2017GL073055>
- 873 Sbar, M. L., & Sykes, L. R. (1973). Contemporary Compressive Stress and Seismicity in Eastern North America: An
874 Example of Intra-Plate Tectonics. *GSA Bulletin*, 84(6), 1861–1882. [https://doi.org/10.1130/0016-7606\(1973\)84<1861:CCSASI>2.0.CO;2](https://doi.org/10.1130/0016-7606(1973)84<1861:CCSASI>2.0.CO;2)
- 876 Suleiman, A. S., Doser, D. I., & Yarwood, D. R. (1993). Source parameters of earthquakes along the coastal margin
877 of West Africa and comparisons with earthquakes in other coastal margin settings. *Tectonophysics*, 222(1),
878 79–91. [https://doi.org/10.1016/0040-1951\(93\)90191-L](https://doi.org/10.1016/0040-1951(93)90191-L)
- 879 Sykes, L. R. (1978). Intraplate seismicity, reactivation of preexisting zones of weakness, alkaline magmatism, and
880 other tectonism postdating continental fragmentation. *Reviews of Geophysics*, 16(4), 621–688.
881 <https://doi.org/10.1029/RG016i004p00621>
- 882 Tabod, C. T., Fairhead, J. D., Stuart, G. W., Ateba, B., & Ntepe, N. (1992). Seismicity of the Cameroon Volcanic
883 Line, 1982–1990. *Tectonophysics*, 212(3), 303–320. [https://doi.org/10.1016/0040-1951\(92\)90297-J](https://doi.org/10.1016/0040-1951(92)90297-J)
- 884 Talwani, P. (2014). Intraplate earthquakes.
- 885 Tchameni, R., Mezger, K., Nsifa, N. E., & Pouclet, A. (2000). Neoproterozoic crustal evolution in the Congo Craton:
886 evidence from K rich granitoids of the Ntem Complex, southern Cameroon. *Journal of African Earth*
887 *Sciences*, 30(1), 133–147. [https://doi.org/10.1016/S0899-5362\(00\)00012-9](https://doi.org/10.1016/S0899-5362(00)00012-9)
- 888 Thiéblemont, D., Castaing, C., Billa, M., Bouton, P., & Pr at, A. (2009). Notice explicative de la carte g ologique et
889 des ressources min rales de la R publique Gabonaise   1/1000000. *Programme Sysmin*, 8, 384.
- 890 Turnbull, R. E., Allibone, A. H., Matheys, F., Fanning, C. M., Kasereka, E., Kabete, J., et al. (2021). Geology and
891 geochronology of the Archean plutonic rocks in the northeast Democratic Republic of Congo. *Precambrian*
892 *Research*, 358, in–press.
- 893 Tuttle, M. P., Schweig, E. S., Sims, J. D., Lafferty, R. H., Wolf, L. W., & Haynes, M. L. (2002). The Earthquake
894 Potential of the New Madrid Seismic Zone. *Bulletin of the Seismological Society of America*, 92(6), 2080–
895 2089. <https://doi.org/10.1785/0120010227>
- 896 Ubangoh, R. U., Ateba, B., Ayonghe, S. N., & Ekodeck, G. E. (1997). Earthquake swarms of Mt Cameroon, West
897 Africa. *Journal of African Earth Sciences*, 24(4), 413–424. [https://doi.org/10.1016/S0899-5362\(97\)00072-9](https://doi.org/10.1016/S0899-5362(97)00072-9)
- 898 Verberne, B. A., Niemeijer, A. R., De Bresser, J. H. P., & Spiers, C. J. (2015). Mechanical behavior and
899 microstructure of simulated calcite fault gouge sheared at 20–600 C: Implications for natural faults in
900 limestones. *Journal of Geophysical Research: Solid Earth*, 120(12), 8169–8196.
901 <https://doi.org/10.1002/2015JB012292>
- 902 Villeneuve, M., & Corn e, J. J. (1994). Structure, evolution and palaeogeography of the West African craton and
903 bordering belts during the Neoproterozoic. *Precambrian Research*, 69(1), 307–326.
904 [https://doi.org/10.1016/0301-9268\(94\)90094-9](https://doi.org/10.1016/0301-9268(94)90094-9)
- 905 Walker, R. T., Telfer, M., Kahle, R. L., Dee, M. W., Kahle, B., Schwenninger, J.-L., et al. (2016). Rapid mantle-
906 driven uplift along the Angolan margin in the late Quaternary. *Nature Geoscience*, 9(12), 909–914.
907 <https://doi.org/10.1038/ngeo2835>

908 Waring, G. A., Blankenship, R. R., & Bentall, R. (1965). *Thermal Springs of the United States and Other Countries:*
 909 *A Summary*. U.S. Government Printing Office.

910 Wiens, D. A., & Stein, S. (1983). Age dependence of oceanic intraplate seismicity and implications for lithospheric
 911 evolution. *Journal of Geophysical Research: Solid Earth*, 88(B8), 6455–6468.

912 Wiens, D. A., & Stein, S. (1985). Implications of oceanic intraplate seismicity for plate stresses, driving forces and
 913 rheology. *Tectonophysics*, 116(1–2), 143–162.

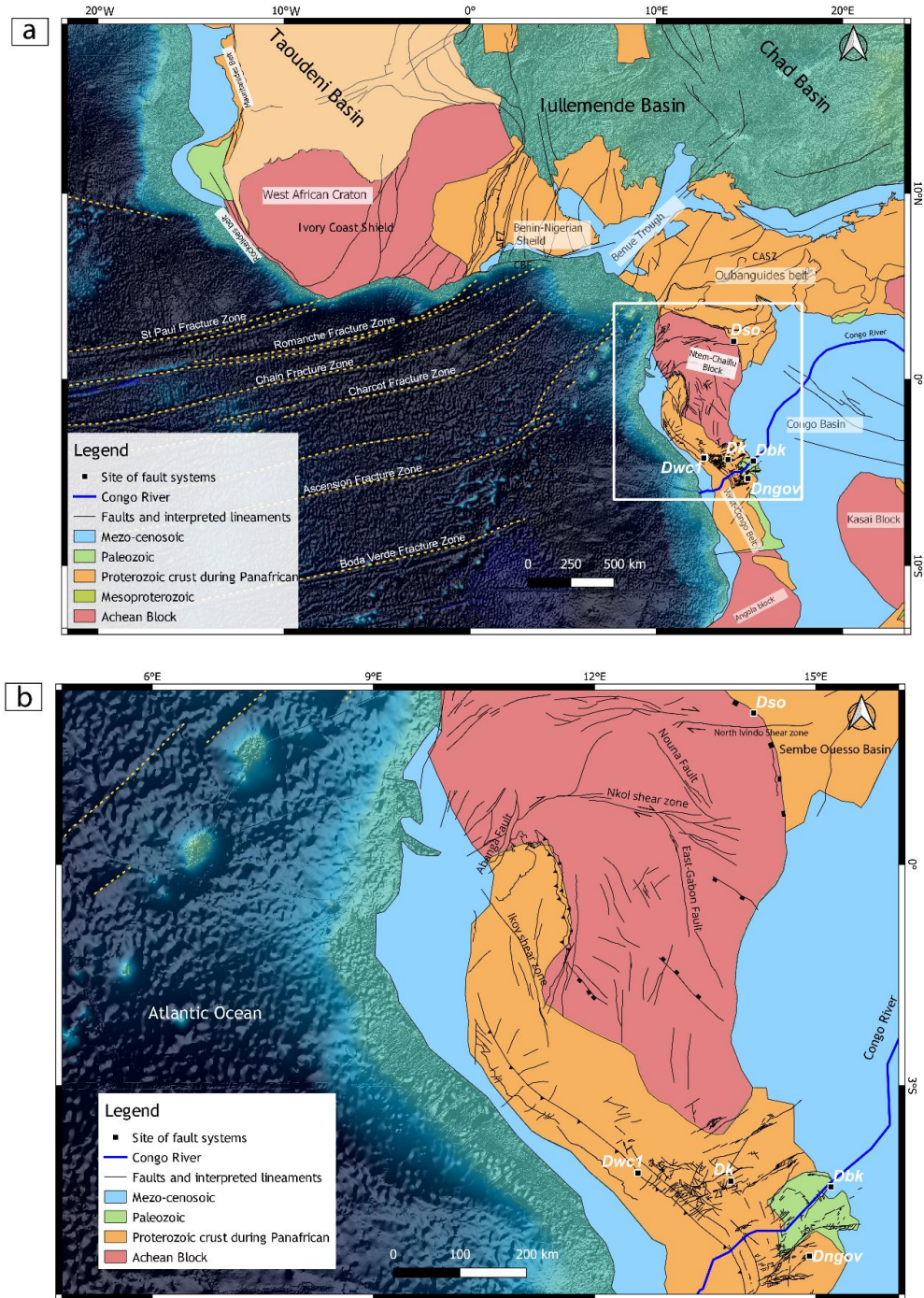
914 Wilson, J. T. (1965). A new class of faults and their bearing on continental drift. *Nature*, 207(4995), 343–347.

915 Woodcock, N. H., & Schubert, C. (1994). Continental strike-slip tectonics. *Continental Deformation*, 251–263.

916 Zoback, M. L. (1992). Stress field constraints on intraplate seismicity in eastern North America. *Journal of*
 917 *Geophysical Research: Solid Earth*, 97(B8), 11761–11782. <https://doi.org/10.1029/92JB00221>

918
 919
 920
 921
 922
 923
 924
 925
 926
 927
 928
 929
 930
 931
 932
 933
 934
 935
 936
 937
 938
 939
 940
 941
 942
 943
 944
 945
 946
 947
 948
 949
 950
 951
 952
 953
 954
 955
 956
 957

958
959
960
961
962
963
964
965
966
967
968
969
970
971
972
973
974
975
976
977
978
979
980
981
982
983
984
985
986
987
988
989
990
991
992
993
994
995
996



997 **Figure 1:** Map of the bedrock geology of the Nubian Plate showing major litho-tectonic
998 subdivisions of the crust. Dwcl, Dk, Dbk, Dngov, Dso represent field sites where structural
999 measurements of fault systems were collected. Dwcl represent the study site of a thrust fault system
1000 in western Congo. Dwcl is a combination of strike-slip faults in Dk and Dngov which represent
1001 field sites in Kolas Quarry, Republic of Congo, and Ngovo Cave, Democratic Republic of Congo
1002 respectively. Dbk represents the field study sites of fault systems in Brazzaville and Kinshasa

1003 areas. AFZ: Akwapim Fault Zone, BFZ: Bouandary Fault Zone, CASZ: Central African shear
 1004 zone.

1005

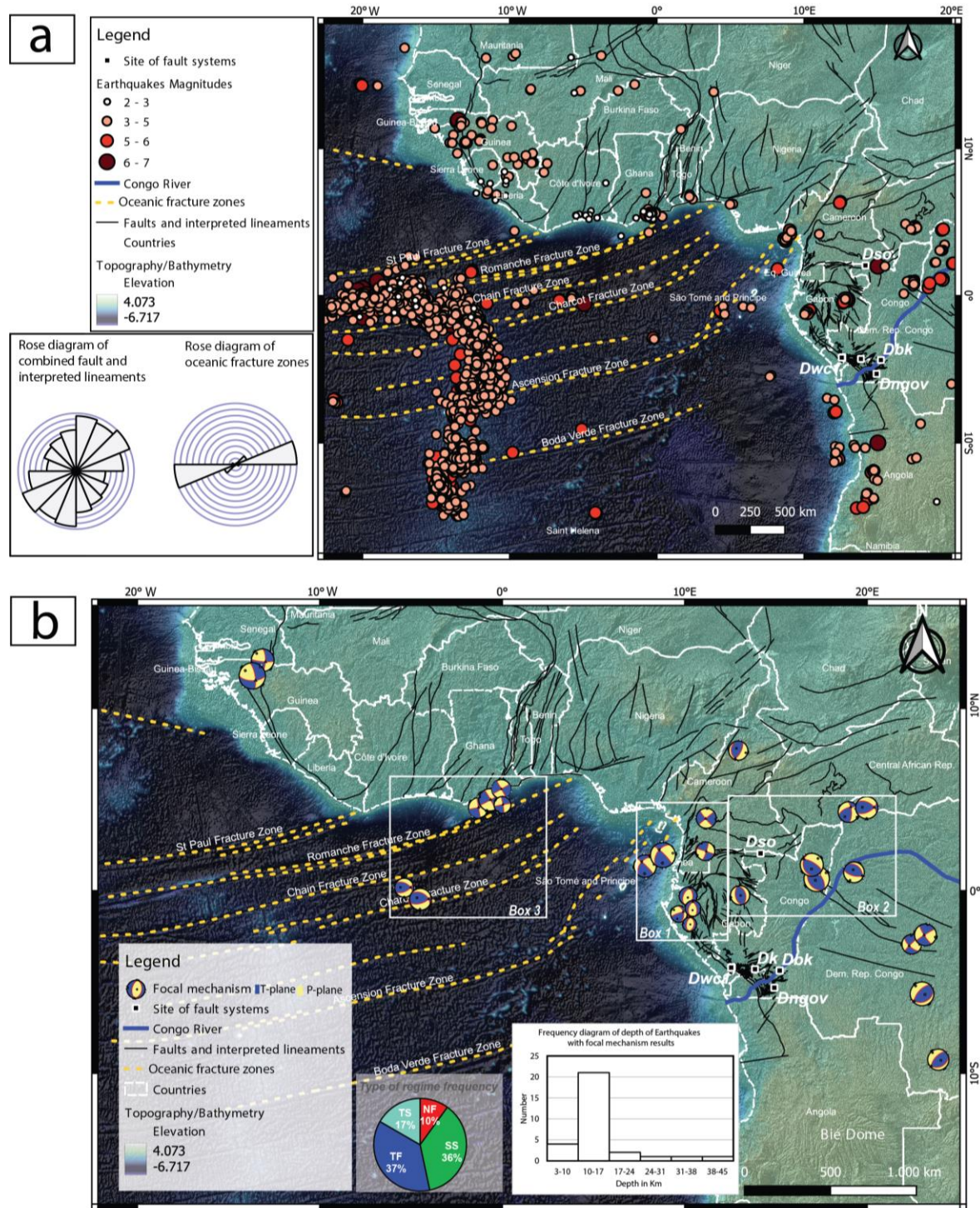
1006

1007

Orientation of horizontal stresses							
Stress ratio- R	0.00	0.25 0.50	0.75 1.00	0.75 0.50	0.25 0.00	0.25 0.50	0.75 1.00
Stress regime	Radial extensional	Pure extensional	Transtensional	Pure strike-slip	Transpressive	Pure compressive	Radial compressive
Stress index -R'	0.00	0.25 0.50	0.75 1.00	1.25 1.50	1.75 2.00	2.25 2.50	2.75 3.00
Determination of R'	R'=R			R'=2-R		R'=2+R	

1008

1009 **Figure 2:** Standard values of the stress index R' with respect to the various tectonic stress regimes
 1010 (modified from Delvaux et al., 2017).



1011

1012 **Figure 3:** (a) Map of the distribution of earthquakes in the Western African passive margin. AFZ,
 1013 CASZ are the Akwapim Fault zone, the Central Africa shear zone. (b) Focal mechanisms solution
 1014 for earthquakes in the western part of the Nubia Plate, obtained from several literature review,
 1015 Global CMT moment tensor, and GFZ GEOFON earthquake catalogs. The boxes show the area
 1016 where conducted stress inversion on focal mechanism results. The pie-chart show the frequency

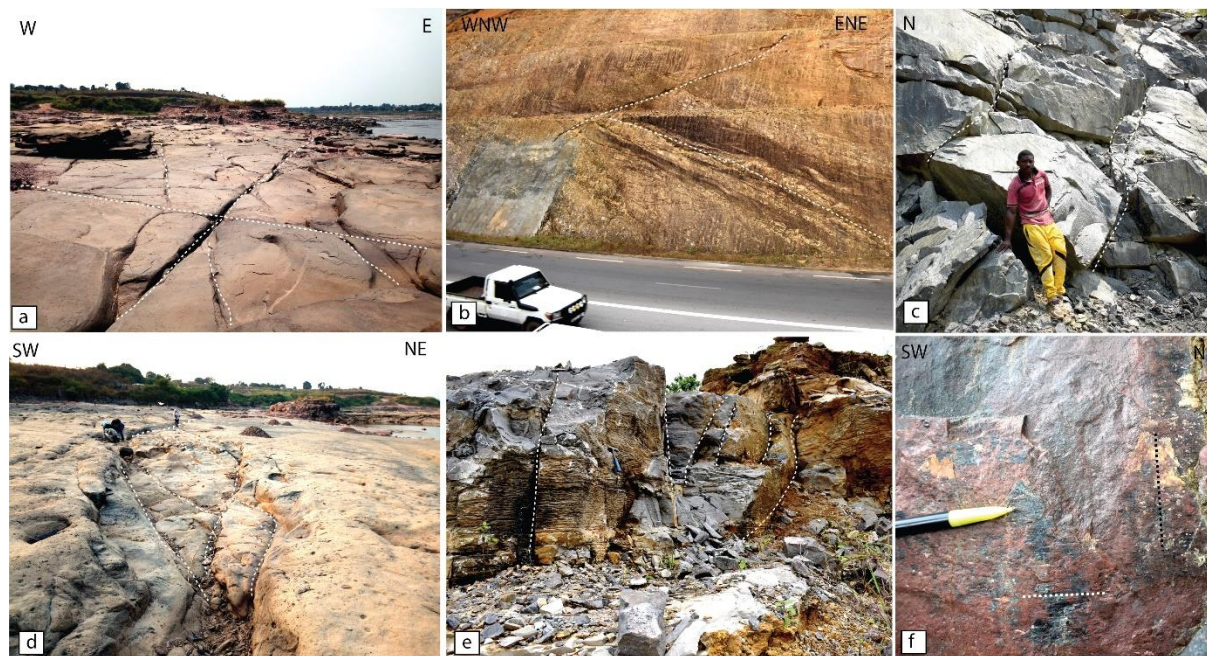
1017 *distribution of the different tectonic regime acting on the area. TS: trenstensional regime; NF:*
 1018 *normal faulting regime; SS: strike-slip faulting regime; TF: thrust faulting regime.*

1019

1020

1021

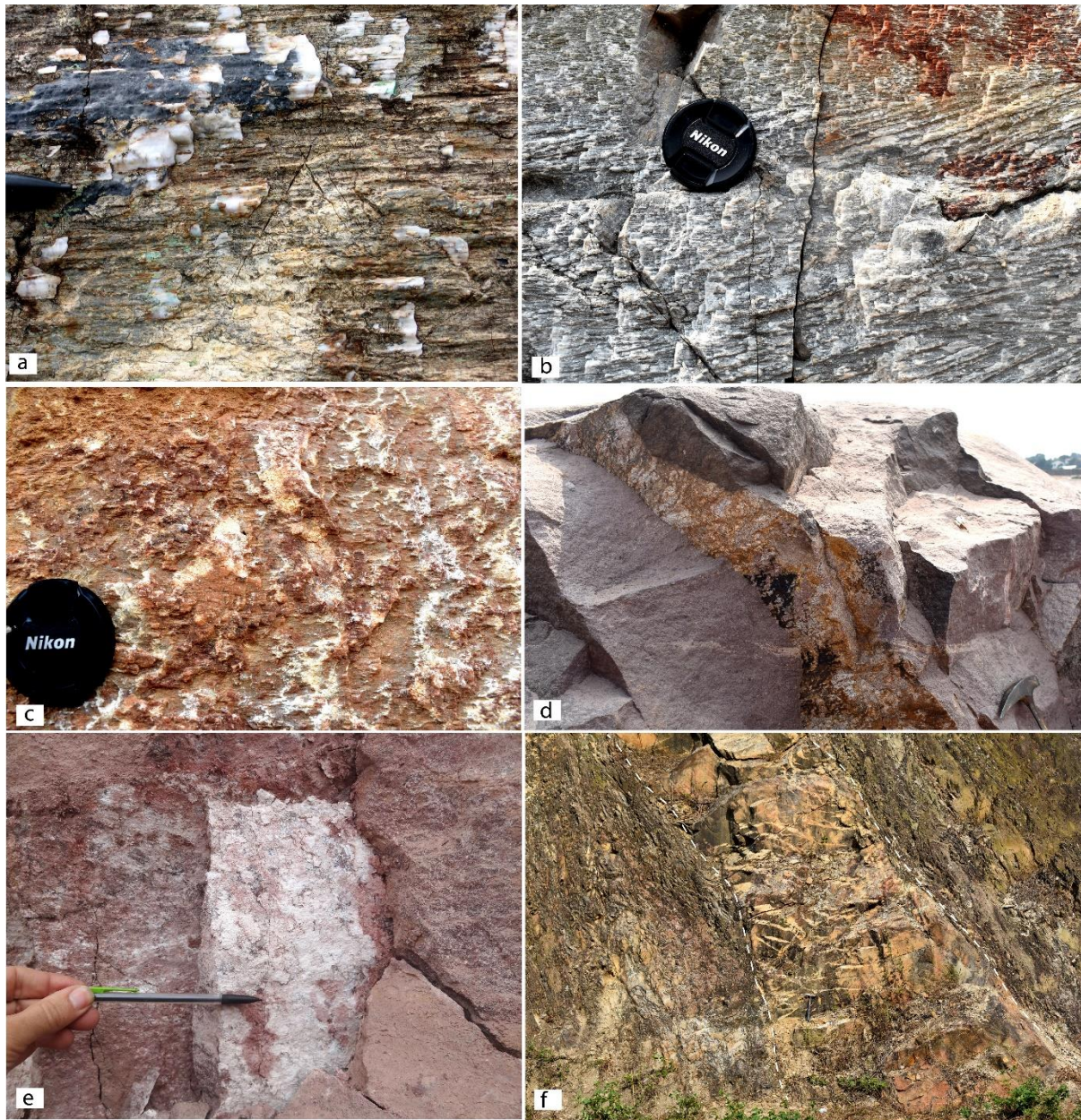
1022



1023

1024 **Figure 4:** *Field observations of faults systems. (a & d) Fault systems in outcrops of the Inkisi*
 1025 *Group (Dbk), showing fracture patterns (highlighted in white dashed line in 3a), and a fault zone*
 1026 *showing segmented faults in a duplex zone (in 3d), at the Kombé quarry, located near the Congo*
 1027 *River, Brazzaville. (b & e) Faults systems (Dwc1 & Dk) in the West-Congo Belt showing*
 1028 *successively thrust and back-thrust affecting schists and quartzites, in Dolisie along the RNI*
 1029 *primary road, and strike-slip fault planes in Kolas quarry near Loutété region. (c & f) Faults*
 1030 *systems (Dso) in Souanké showing high-angle planes of strike-slip faults in the area (in 3c) and, a*
 1031 *NE-trending plane that shows horizontal striae that is over-printed by vertical striae associated*
 1032 *with calcite fibers, indicating a later normal faulting reactivation of the strike-slip faults. The*
 1033 *dashed lines in Fig. 3f represent the directions of striae.*

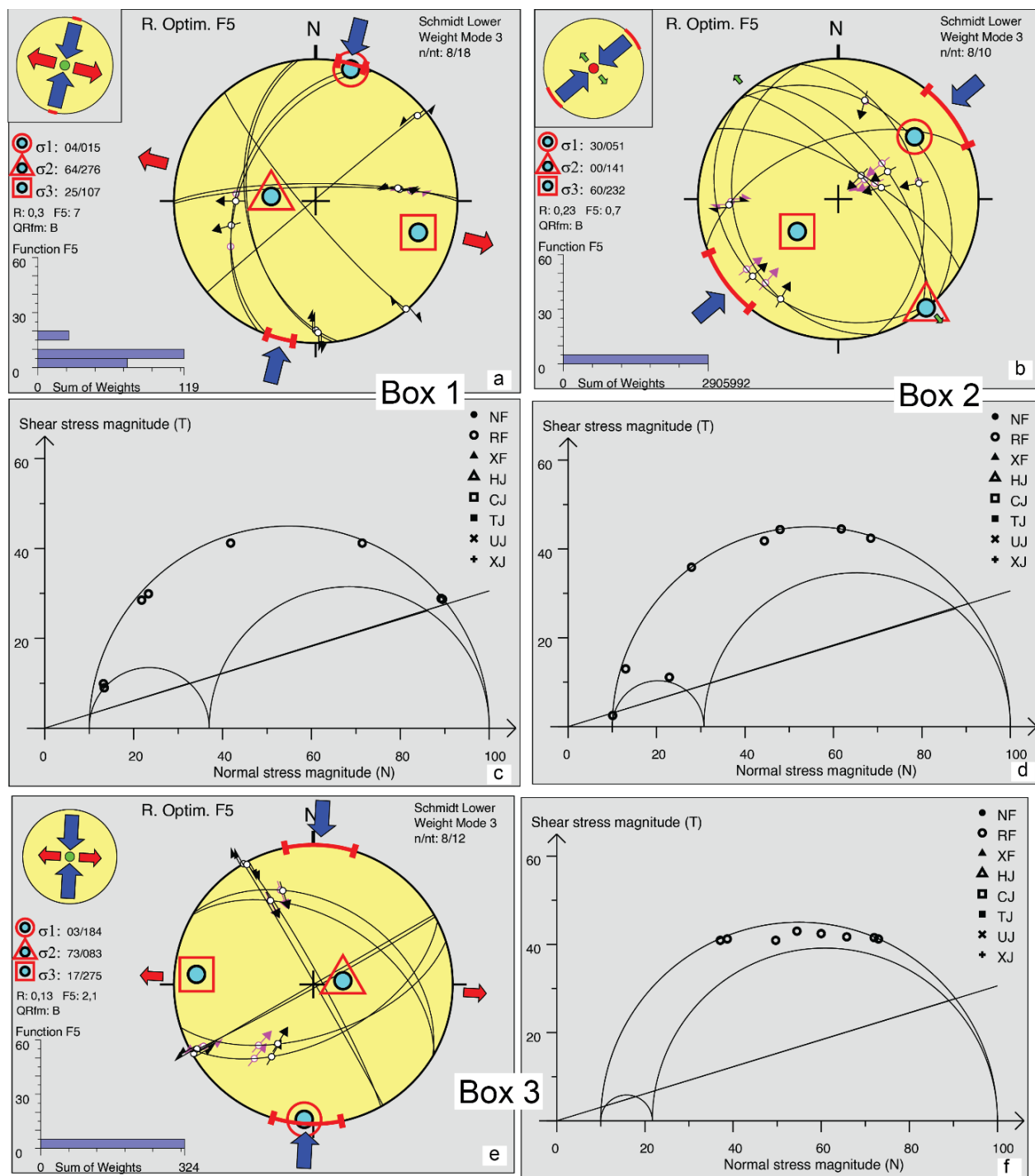
1034



1035

1036 **Figure 5:** *Geochemical alterations along mineralized fault surfaces. (a) Accretion calcite steps*
 1037 *along NW-SE strike-slip faults in carbonates rocks of the West Congo Belt, DRC. (b - c)*
 1038 *Carbonate-hosted fault surfaces covered by accretion calcite steps and iron staining. Note that the*
 1039 *carbonate rock in Figure 5b has penetrative cross-bedding structures that should not be confused*
 1040 *with slickenlines. (d) Fault surface in Inkisi sandstones associated with iron alteration realm. (e)*
 1041 *Slickensided palygorskite along a fault in Dbk fault system. (f) Deformed doleritic intrusion along*
 1042 *a high-angle thrust-fault (230/40) injected with quartz veins in the Dwcl fault system.*

1043

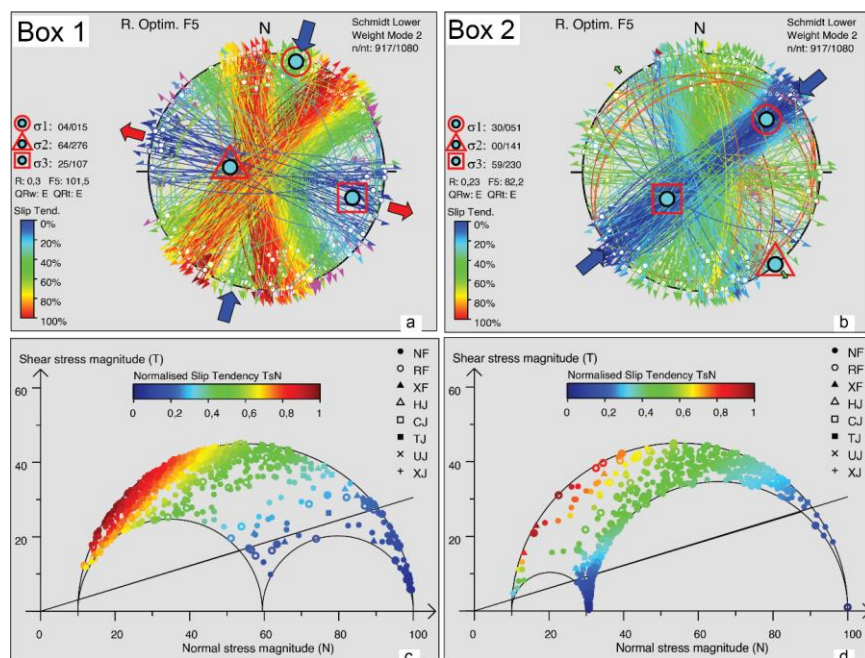


1044

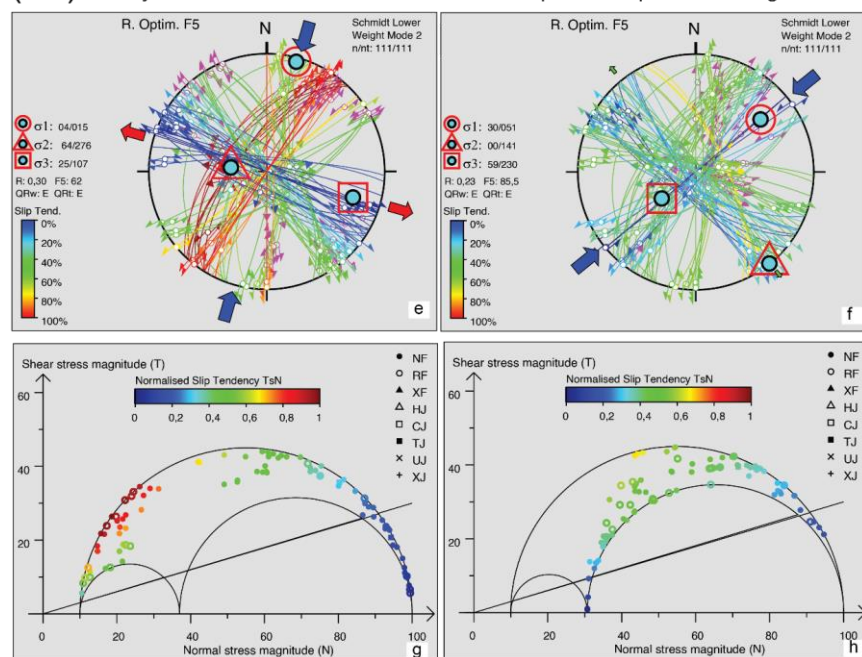
1045 **Figure 6:** Results of stress tensors from the inversion of earthquake focal mechanism solution
 1046 along the western Africa continental margin, offshore and onshore Gulf of Guinea represented by
 1047 sub-regional boxes (see Fig. 3b).

1048

(Dbk) Faults systems in the inkisi Group



(Dso) fault system in archean rocks in the Ivindo complex in Republic of Congo



1049

1050 **Figure 7:** The application of the stress inversion results for Box 1 (left column) and Box 2 (right
 1051 column) on Dbk and Dso fault systems and the resulting Slip Tendency values associated with their
 1052 Mohr-Coulomb stress states. The slip tendency estimate associated with each fault segment is
 1053 presented as color-coded planes in both the stereoplots and their adjoining Mohr diagrams.

1054

1055

1056

1057

1058 **Table 1:** Stress parameters associated with the focal mechanism solution of earthquakes in Box 1,
 1059 Box 2, and Box 3 in Figure 2b. *n*: number of data used, *nt*: total data, *Pl* & *Az*: plunge & azimuth
 1060 of principal compressive stress tensors, *R'*: index regime; *Reg*: Regime, *QRfm*: Quality rank of
 1061 focal mechanism.

Stress parameters	<i>n</i>	<i>nt</i>	$\sigma 1$		$\sigma 2$		$\sigma 3$		<i>Reg</i>	<i>QRfm</i>	<i>R'</i>		<i>Shmax</i>	<i>Shmin</i>
			<i>Pl</i>	<i>Az</i>	<i>Pl</i>	<i>Az</i>	<i>Pl</i>	<i>Az</i>			Value	meaning		
Box 1- West Central	8	18	4	15	64	276	25	107	SS	B	1.75	Transpressive	14	102
Box 2- Continental interior	8	10	30	51	0	141	60	232	TF	B	2.2	Transpressive	49	40
Box 3- Western Coastal Margin	8	12	3	184	73	83	17	275	SS	B	1.87	Transpressive	3	93

1062